JOURNAL OF PETROLOGY | VOLUME 45 | NUMBER 1 | PAGES 183–202 | 2004 | DOI: 10.1093/petrology/egg085

Calculated Phase Relations in High-Pressure Metapelites in the System NKFMASH (Na_2O–K_2O–FeO–MgO–Al_2O_3–SiO_2–H_2O)

CHUNJING WEI[1]* AND ROGER POWELL[2]

[1]SCHOOL OF EARTH AND SPACE SCIENCES, BEIJING UNIVERSITY, BEIJING 100871, P.R. CHINA

[2]SCHOOL OF EARTH SCIENCES, THE UNIVERSITY OF MELBOURNE, VIC. 3010, AUSTRALIA

RECEIVED FEBRUARY 20, 2002; ACCEPTED MARCH 21, 2003

Using an internally consistent thermodynamic dataset and updated models of activity–composition relation for solid solutions, petrogenetic grids in the system NKFMASH (Na_2O–K_2O–FeO–MgO–Al_2O_3–SiO_2–H_2O) and the subsystems NKMASH and NKFASH have been calculated with the software THERMOCALC 3.1 in the P–T *range 5–36 kbar and 400–810°C, involving garnet, chloritoid, biotite, carpholite, talc, chlorite, kyanite/sillimanite, staurolite, phengite, paragonite, albite, glaucophane, jadeite, with quartz/coesite and H_2O in excess. These grids, together with calculated AFM compatibility diagrams and* P–T *pseudosections, are shown to be powerful tools for delineating the phase equilibria and* P–T *conditions of Na-bearing pelitic assemblages for a variety of bulk compositions from high-*P *terranes around the world. These calculated equilibria are in good agreement with petrological studies. Moreover, contours of the calculated phengite Si isopleths in* P–T *pseudosections for different bulk compositions confirm that phengite barometry is highly dependent on mineral assemblage.*

KEY WORDS: *phase relations; HP metapelite; NKFMASH; THERMOCALC; phengite geobarometry*

INTRODUCTION

In the last decade, the use of internally consistent thermodynamic databases (Holland & Powell, 1990, 1998) has led to the construction of quantitative petrogenetic grids for the model system KFMASH system (K_2O–FeO–MgO–Al_2O_3–SiO_2–H_2O) that have greatly extended the applicability of such model systems to natural rock assemblages for low- and medium-*P* metamorphism (e.g. Powell & Holland, 1990; Xu *et al*., 1994) and also for model systems involving partial melting (White *et al*., 2001). Wei & Powell (2003) have calculated such a petrogenetic grid for high-*P* metapelites in the KFMASH system with the mineral phases garnet, chloritoid, chlorite, biotite, carpholite, talc, staurolite, kyanite with phengite, quartz/coesite and H_2O in excess. With this grid, the high-*P* phase relations in the KFMASH system, the typical whiteschist parageneses kyanite–talc and talc–phengite (Schreyer, 1973, 1977, 1988; Chopin, 1981) in the KMASH subsystem and phengite geobarometry relationships (Massonne & Schreyer, 1989; Massonne & Szpurka, 1997) in KMASH and KFMASH have been documented for a variety of bulk compositions from several typical high-*P* terranes. However, Na-bearing metapelites occur widely, as have been reported from high-*P* terranes around the world, commonly containing one or more of the Na phases paragonite, glaucophane, jadeite and albite in addition to the above KFMASH phases. Examples are the mineral assemblages chloritoid + talc + chlorite + phengite + quartz + glaucophane ± garnet described by Chopin (1981) from the Gran Paradiso terrane, Western Alps; garnet + phengite + kyanite + quartz + paragonite reported by Meyre *et al*. (1999) in the Adula Nappe, Central Alps; chloritoid + carpholite + chlorite + phengite + quartz + paragonite described by Theye *et al*. (1992) in the Peloponnese, Greece; garnet + chlorite + paragonite + glaucophane + phengite + quartz and garnet + chlorite + paragonite + chloritoid + phengite + quartz observed in New Caledonia

*Corresponding author. Telephone: 86-10-62754157. Fax: 86-10-62751159. E-mail: cjwei@pku.edu.cn

Journal of Petrology 45(1) © Oxford University Press 2004; all rights reserved

Downloaded from http://petrology.oxfordjournals.org/ at Pennsylvania State University on March 5, 2016

by Yokoyama *et al.* (1986) and Ghent *et al.* (1987), in Alaska by Brown & Forbes (1986), in Vendée by Guiraud *et al.*, (1987), and in Sesia, Western Alps, by Vuichard & Ballèvre (1988); the coexistence of chloritoid–glaucophane reported in Ile de Groix (Kiénast & Triboulet, 1972), in and around the Gran Paradiso massif, Western Alps (Chopin, 1981), in Spitsbergen (Ohta *et al.*, 1986), in Oman (El-Shazly & Liou, 1991) and in Chinese Tianshan (L. F. Zhang, personal communication, 2002); garnet + phengite + quartz + glaucophane + jadeite + paragonite observed by Koons (1986) in the Sesia–Lanzo zone, Western Alps; and the talc–phengite–albite assemblage confirmed by Izadyar *et al.* (2000) in the Sanbagawa belt, Japan; and so forth. Whether and how do these Na phases affect the KFMASH phase relations? What are the phase topologies in the NKFMASH system? In addition, Wei & Powell (2003) have extended the experimentally calibrated phengite geobarometry (Massonne & Schreyer, 1989; Massonne & Szpurka, 1997) to various KFMASH parageneses: is this geobarometric method applicable to NKFMASH assemblages?

In this paper, petrogenetic grids in the model system NKFMASH and the subsystems NKMASH and NKFASH are calculated in the P–T range 5–36 kbar and 400–810°C, involving combinations of garnet, chloritoid, biotite, carpholite, talc, chlorite, staurolite, phengite, paragonite, glaucophane, jadeite, albite, kyanite/sillimanite with quartz/coesite and H_2O in excess. In constructing these grids, we adopted the internally consistent dataset of Holland & Powell (1998), the software THERMOCALC 3.1 (Powell *et al.*, 1998) and updated models of activity–composition relationships for solid solutions; ideal mixing models are used for phengite, glaucophane, talc and carpholite, symmetric mixing models for garnet, chloritoid, staurolite and symmetric mixing, and Darken's quadratic formulism (DQF) models (Powell, 1987) for ordered chlorite, biotite and albite (for details see the Appendix).

PETROGENETIC GRIDS

The calculated P–T projections in the subsystems NKMASH and NKFASH and the full system NKFMASH are presented in Figs 1–3, and calculated results for the invariant points are tabulated in Tables 1–3.

NKMASH grid

In the subsystem NKMASH grid (Fig. 1), there are 17 invariant points stable in the P–T range of interest involving the phases biotite, chlorite, talc, Mg-carpholite, kyanite, phengite, albite, glaucophane, paragonite, jadeite (+ quartz/coesite + H_2O). The invariant points involving one Na phase such as mi1 and mi2, and the univariant lines emanating from them, are the same as those in KMASH (Wei & Powell, 2003). These KMASH univariants are shown as bold lines in Fig. 1. The invariant points involving two Na-bearing phases appear on these KMASH univariant lines and the invariant points containing three or more Na-bearing phases occur between these KMASH univariant lines. This NKMASH grid defines the maximum stability fields of some of the Mg- and/or Na-bearing endmembers. For example, in the presence of quartz, reactions m1 (chl = ta + ky) and m3 (chl = ta + mcr) define the maximum stability of Mg-chlorite, and reactions m4 (mcr = chl + ky) and m5 (mcr = ta + ky) limit the stability of Mg-carpholite. The stability fields of paragonite, albite and jadeite are defined by the NASH reactions n1 (pa = ab + ky), n2 and n3 (jd + q = ab). Glaucophane can be stable over a wide range in the higher-pressure part of Fig. 1 with its lower-P limit defined by reactions m6 (gl + chl = ta + ab), m7 (gl + ph = bi + ta + ab), m8 (gl + pa = ta + ab) and m9 (gl + ky = ta + ab), which, in P–T conditions, are analogous to the classical NMASH reaction gl + q = ta + ab (Holland, 1988). The higher-P limit of glaucophane is restricted by reactions m15 (ky + gl = ta + jd) and m16 (mcr + gl = ta + jd), corresponding to the classical NMASH reaction gl + q = ta + jd (Holland, 1988). These classical NMASH reactions do not appear in our study because of the Tschermak substitution in talc.

In the KMASH subsystem, the characteristic paragenesis for whiteschist ta + ky occupies a wide P–T field bounded by reactions m1, m5 and m10 (ta + ph = bi + ky) on the lower P–T sides, and by reaction m11 (ta + ky = py + coe) on the higher P–T side. However, in the NKMASH subsystem and with paragonite in excess, the paragenesis ta + ky has a reduced field and, with pressure increasing, gives way to gl–ky through reaction m12 (ta + pa = gl + ky).

In the NKMASH subsystem, jadeite could coexist with MASH phases such as Mg-carpholite at pressures over 20–25 kbar (reaction m13, mcr + jd = gl + pa) and temperatures below 550–580°C (reaction m14, mcr + jd = gl + ky), and with Mg-talc only at pressures over 35–36 kbar (reactions m15 and m16). At lower pressures, jadeite could coexist with Na phases such as glaucophane and paragonite, but could not coexist with any other MASH members. From Fig. 1, the paragenesis pa + bi is bounded by reactions m21, m22, m23 and n1, being stable only at medium P–T.

NKFASH grid

The calculated P–T projection for NKFASH is displayed in Fig. 2. There are 20 stable invariant points involving the phases biotite, chlorite, almandine,

Downloaded from http://petrology.oxfordjournals.org/ at Pennsylvania State University on March 5, 2016

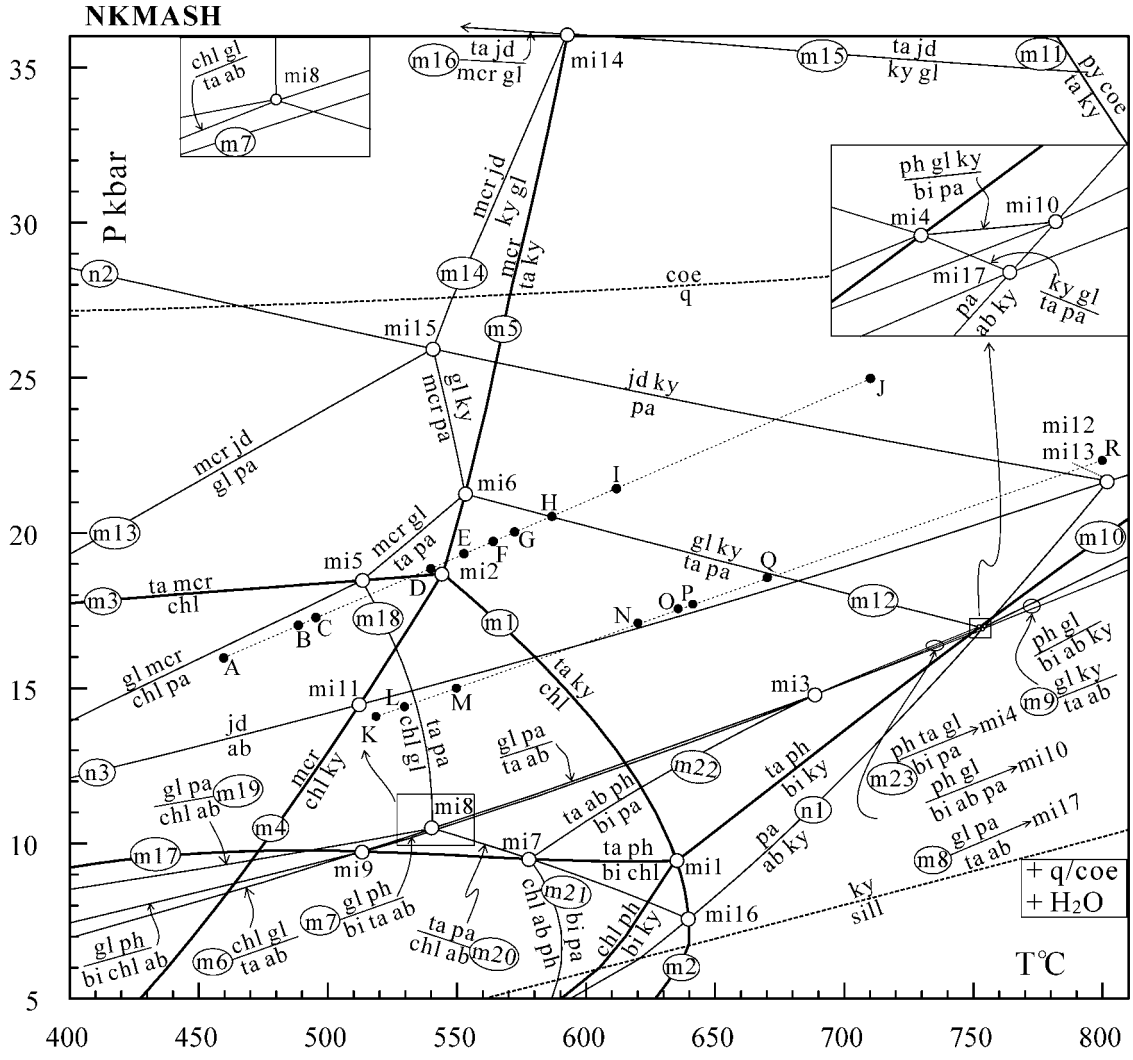

Fig. 1. *P–T* projection for the subsystem NKMASH in projection from quartz/coesite and H_2O. Labels mi1–mi17 refer to the invariant points in NKMASH. Labels m1–m23, and n1–n3 (shaded circles) refer to the univariant reactions discussed in the text. Invariant points mi12 and mi13 are plotted on the same location because of the system degeneracy. Bold lines represent the univariant reactions that are the same as those in the KMASH system. The reactions coe = q and ky = sill are shown as bold dashed lines. Black dots with letters A–R are *P–T* locations of the AFM compatibility diagrams shown in Figs 4 and 5. ab, albite; bi, biotite; chl, chlorite; coe, coesite; gl, glaucophane; jd, jadeite; ky, kyanite; mcr, Mg-carpholite; pa, paragonite; ph, phengite; py, pyrope; q, quartz; ta, talc; sill, sillimanite.

Fe-chloritoid, Fe-carpholite, talc, Fe-staurolite, phengite, Fe-glaucophane, paragonite, kyanite/sillimanite, albite and jadeite + (quartz/coesite + H_2O). Like those in NKMASH, the invariant points in NKFASH involving one Na phase such as fi1, fi2, fi3 and fi20 and the univariant lines emanating from them coincide with those in KFASH (Wei & Powell, 2003). These KFASH univariant lines are displayed as bold lines in Fig. 2. The invariant points involving two Na phases appear on these KFASH lines, and the invariant points containing three or more Na phases occur between them. The NKFASH grid defines the maximum stabilities of some of the Fe- and/or Na-bearing end-members. For example, reactions f1 (chl + fct = alm) and f4 (chl + fcr = alm) mark the low-*T* limit of almandine; reactions f15 (fct + ky = fst) and f16 (fst = alm + ky/sill) limit the stability field of Fe-staurolite; and reactions f3 (fct = alm + ky), f14 (fct = alm + fst) and f5 (fcr = fct) restrict the stability field of Fe-chloritoid. If phengite is in excess, reactions f2 (ph + chl = bi + alm) and f19 (ph + chl = bi + fct) give the high-*T* limit of Fe-chlorite, and if phengite is absent, Fe-chlorite will be stable up to reaction f6 (chl = alm + ta). The stability fields of paragonite, albite and jadeite are defined by the NASH reactions n1, n2 and n3. In the presence of phengite, reactions f7 (fgl + ph = bi + chl + ab), f8 (fgl +ph = bi + ab + pa), f9 (fgl + ph = bi + ab + alm) and f10 (fgl + ph = bi + alm + jd)

Downloaded from http://petrology.oxfordjournals.org/ at Pennsylvania State University on March 5, 2016

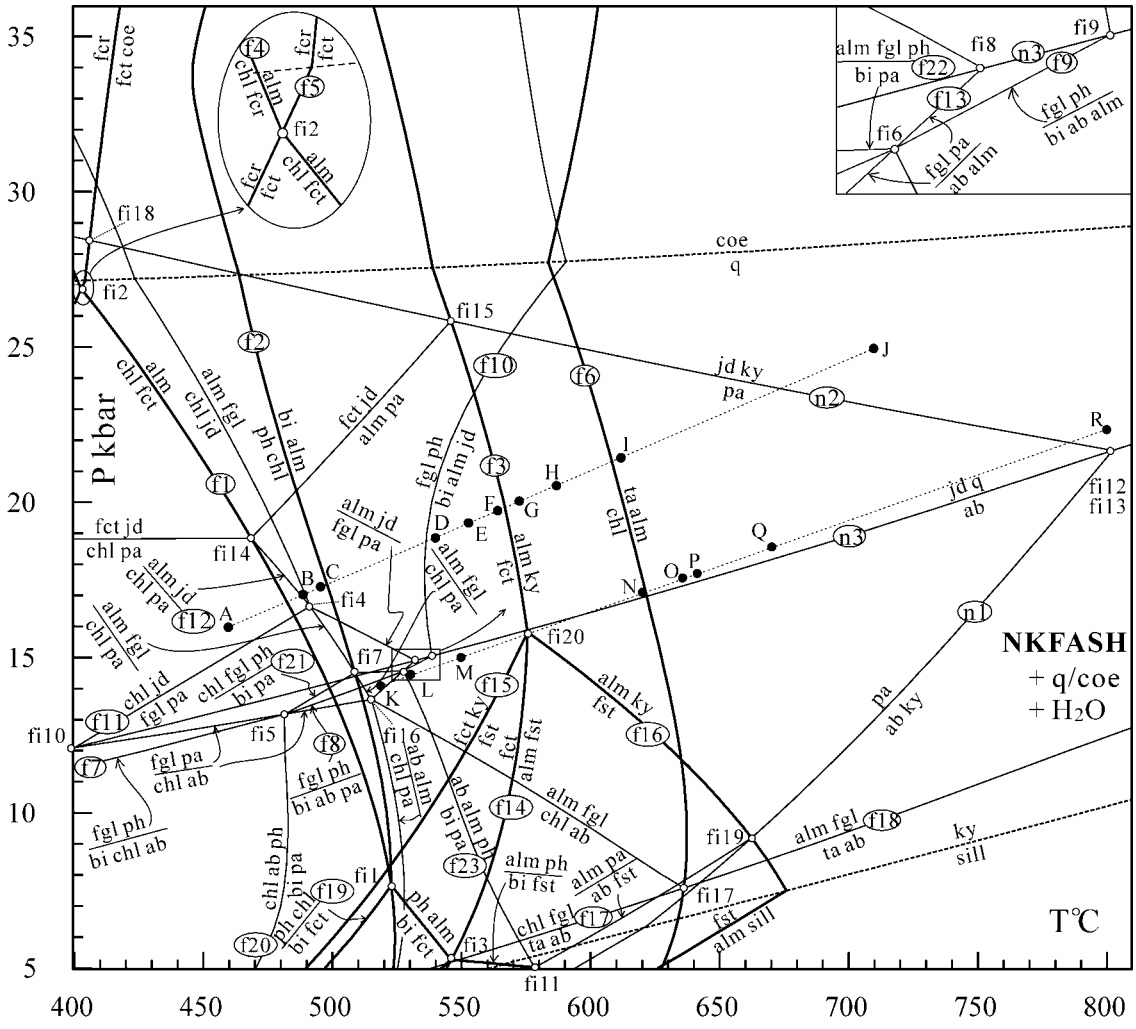

Fig. 2. *P–T* projection for the subsystem NKFASH in projection from quartz/coesite and H_2O. Labels fi1–fi20 refer to the invariant points in the NKFASH. Labels f1–f23 and n1–n3 in the shaded circles refer to the univariant reactions considered in the text. Invariant points fi12 and fi13 are plotted at the same location because of the system degeneracy. Bold lines represent the univariant reactions that are the same as those in the KFASH system. alm, almandine; fcr, Fe-carpholite; fct, Fe-chloritoid; fgl, Fe-glaucophane; fst, Fe-staurolite. Other abbreviations are as in Fig. 1.

define the stability of Fe-glaucophane to be above 11–15 kbar and below about 540–580°C. However, when phengite is absent, Fe-glaucophane can be stable at much lower pressures, defined by reactions f17 (chl + fgl = ta + ab) and f18 (alm + fgl = ta + ab). Unlike in the NKMASH subsystem, jadeite can coexist with many of the KFASH phases such as Fe-chlorite, almandine, Fe-biotite and Fe-chloritoid.

NKFMASH grid

The full system NKFMASH grid is shown in Fig. 3 and the calculated results for the stable invariant equilibria are listed in Table 3. There are 31 invariant points stable in the *P–T* range of interest, denoted by filled circles with labels i1–i31. The full system univariant curves terminate at the NKMASH and NKFASH subsystem invariant points denoted, respectively, by shaded and white circles.

Like those in the NKMASH and NKFASH subsystems, the invariant equilibria in the full system involving one Na phase such as the points i1–i6, i30 and i31 and the univariant lines emanating from them are the same as those in KFMASH (Wei & Powell, 2003); that is, incorporation of Na does not change the basic framework of the KFMASH grid. These KFMASH univariant lines, displayed as bold lines in Fig. 3, constrain stability fields of the KFMASH phases free of Na. For example, the stability of chlorite is confined by reactions 1 and 2 (chl = g + ta + ky/sill) to be at pressures below invariant point i3, stable at higher temperatures than chloritoid, but at pressures above i3, chlorite is

Downloaded from http://petrology.oxfordjournals.org/ at Pennsylvania State University on March 5, 2016

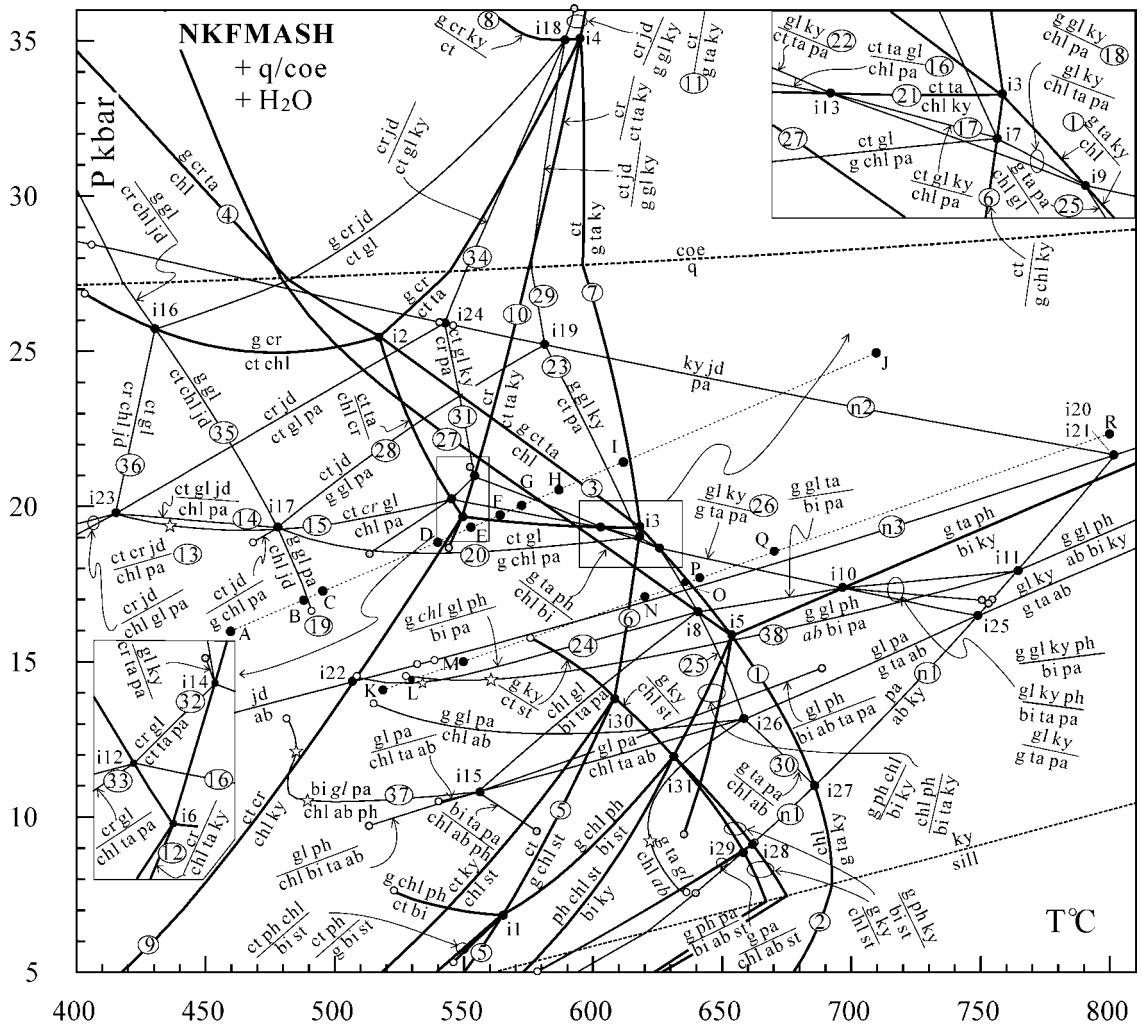

Fig. 3. *P–T* projections for the full system NKFMASH in projection from quartz/coesite and H_2O. Labels i1–i31 refer to the invariant points in NKFMASH. Labels 1–38 and n1–n3 in the shaded circles refer to the univariant reactions discussed in the text. Invariant points i20 and i21 are plotted at the same location because of the system degeneracy. Bold lines represent the univariant reactions that are the same as those in the KFMASH system. Full system reactions terminating at the KMASH and KFASH subsystem invariant points are shown by shaded and unshaded circles, respectively, with the subsystem reactions omitted for clarity. Unfilled stars indicate the location of singularities, and the phases that 'swap' sides of the reaction are shown in italics. cr, carpholite; ct, chloritoid; g, garnet; st, staurolite. Other abbreviations are as in Figs 1 and 2.

limited by reactions 3 (chl = g + ta + ct) and 4 (chl = g + ta + cr), stable at lower temperatures than chloritoid. With the presence of quartz/coesite, chloritoid breaks down via reactions 5 (ct = g + chl + st), 6 (ct = g + chl + ky), 7 (ct = g + ta + ky) and 8 (ct = g + cr + ky), which, at pressures below i4, are good temperature indicators. The maximum stability of carpholite is confined by reactions 9 (cr + ct = chl + ky), 10 (cr = ct + ta + ky), 11 (cr = g + ta + ky) and 12 (cr = chl + ta + ky), almost in the same position as in NKMASH.

The invariant points containing two Na phases appear on the KFMASH univariant lines, and the invariant points involving three or more Na phases plot between these KFMASH lines. As in the NKMASH and NKFASH subsystems, the NASH reactions n1–n3 constrain the maximum stabilities of paragonite, jadeite and albite.

Generally, incorporation of Na phases leads to a reduction in the stability fields of the KFMASH phases free of Na. For example, if paragonite is in excess, chlorite will be consumed at lower pressures of about 18–20 kbar, through a series of reactions with flat slopes, i.e. reactions 13 (chl + pa = ct + cr + jd), 14 (chl + pa = ct + gl + jd), 15 (chl + pa = ct + cr + gl), 16 (chl + pa = ct + ta + gl), 17 (chl + pa = ct + gl + ky) or 18 (chl + pa = g + gl + ky), and the reactions 1, 3 and 4 confining the maximum stability of chlorite will not occur. At pressures between invariant points i9

Downloaded from http://petrology.oxfordjournals.org/ at Pennsylvania State University on March 5, 2016

Table 1: Calculated results for stable invariant equilibria in the subsystem NKMASH

Number	Phases (+ q/coe + H_2O)	P (kbar)	T (°C)	y(ph)*	y(bi)	y(chl)	N(chl)	y(ta)	Q(ab)
mi1	ph, bi, chl, ta, ky, pa	9·43	635·1	0·861	0·347	0·545	0·455	0·092	
mi2	ph, chl, ta, mcr, ky, pa	18·68	544·4	0·730		0·519	0·481	0·041	
mi3	ph, bi, ta, ab, gl, pa	14·80	689·1	0·727	0·174			0·067	0·450
mi4	ph, bi, ta, ky, gl, pa	16·96	752·4	0·725	0·201			0·080	
mi5	ph, chl, ta, mcr, gl, pa	18·47	513·3	0·678		0·511	0·489	0·030	
mi6	ph, ta, mcr, ky, gl, pa	21·27	553·1	0·677				0·036	
mi7	ph, bi, chl, ta, ab, pa	9·50	578·4	0·793	0·184	0·517	0·483	0·056	0·697
mi8	ph, chl, ta, ab, gl, pa	10·49	540·4	0·725		0·509	0·491	0·037	0·756
mi9	ph, bi, chl, ta, ab, gl	9·74	513·0	0·681	0·068	0·505	0·495	0·028	0·788
mi10	ph, bi, ab, ky, gl, pa	16·99	754·2	0·725	0·201				0·149
mi11	ph, chl, ab, mcr, ky, jd	14·47	512·2	0·841		0·530	0·470		0·800
mi12	ph, ta, ab, ky, pa, jd	21·67	802·2	0·647				0·072	0·102
mi13	ph, ab, ky, gl, pa, jd	21·67	802·2	0·694					0·102
mi14	ph, ta, mcr, ky, gl, jd	36·20	586·9	0·404				0·017	
mi15	ph, mcr, ky, gl, pa, jd	25·93	540·7	0·633					
mi16	bi, chl, ta, ab, ky, pa	7·56	639·7		0·393	0·552	0·448	0·102	0·559
mi17	bi, ta, ab, ky, gl, pa	16·94	753·7		0·201			0·080	0·150

*$y(ph) = x_{Al}^{M2A}$, $y(bi) = x_{Al}^{M1}$, $y(chl) = x_{Al}^{T1}$, $N(chl) = (x_{Al}^{M4} - x_{Al}^{M1})/2$, $y(ta) = x_{Al}^{M3}$, $Q(ab) = x_{Al}^{T1o} - x_{Al}^{T1m+T2}$.

Table 2: Calculated results of the invariant equilibria in the subsystem NKFASH

Number	Phases (+ q/coe + H_2O)	P (kbar)	T (°C)	y(ph)*	y(bi)	y(chl)	N(chl)	y(ta)	Q(ab)
fi1	ph, bi, chl, alm, fct, pa	7·65	522·7	0·874	0·487	0·545	0·455		
fi2	ph, chl, alm, fct, fcr, jd	26·88	402·8	0·284		0·501	0·499		
fi3	ph, bi, alm, fct, fst, pa	5·27	546·0	0·939	0·685				
fi4	ph, chl, alm, fgl, pa, jd	16·64	491·3	0·547		0·505	0·495		
fi5	ph, bi, chl, ab, fgl, pa	13·16	481·3	0·570	0·068	0·504	0·496		0·829
fi6	ph, bi, ab, alm, fgl, pa	14·56	527·6	0·570	0·086				0·783
fi7	ph, bi, chl, alm, fgl, pa	14·50	508·7	0·570	0·080	0·506	0·494		
fi8	ph, ab, alm, fgl, pa, jd	14·91	532·2	0·566					0·778
fi9	ph, bi, ab, alm, fgl, jd	15·05	538·4	0·547	0·078				0·771
fi10	ph, chl, ab, fgl, pa, jd	12·09	399·1	0·542		0·502	0·498		0·894
fi11	ph, bi, ab, alm, fst, pa	5·02	578·2	0·942	0·703				0·681
fi12	ph, bi, ab, ky, pa, jd	21·67	802·2	0·627	0·258				0·102
fi13	ph, ab, alm, ky, pa, jd	21·67	802·2	0·796					0·102
fi14	ph, chl, alm, fct, pa, jd	18·84	468·5	0·554		0·505	0·495		
fi15	ph, alm, fct, ky, pa, jd	25·84	545·9	0·723					
fi16	bi, chl, ab, alm, fgl, pa	13·65	515·1		0·084	0·506	0·494		0·795
fi17	bi, chl, ta, ab, alm, fgl	7·58	636·1		0·001	0·445	0·445	0·005	0·569
fi18	ph, fct, fcr, ky, pa, jd	28·44	405·9	0·831					
fi19	ph, ab, alm, ky, pa, fst	9·19	662·4	0·919					0·501
fi20	ph, pa, alm, fct, ky, fst	15·82	575·5	0·861					

*Composition variables are as in Table 1.

Downloaded from http://petrology.oxfordjournals.org/ at Pennsylvania State University on March 5, 2016

Table 3: Calculated results for stable invariant equilibria for the system NKFMASH

Number	Phases (+ q/coe + H_2O)	*P* (kbar)	*T* (°C)	x(g)*	x(ct)	x(ph)	y(ph)	x(chl)	y(chl)	N(chl)	x(bi)	y(bi)	Q(bi)	x(st)	x(cr)	x(ta)	y(ta)	x(gl)	Q(ab)
i1	g, ct, chl, bi, pa, st, ph	6·85	565·1	0·935	0·860	0·665	0·907	0·677	0·606	0·394	0·759	0·521	0·123	0·937					
i2†	g, ct, chl, cr, ta, gl, ph	25·47	517·2	0·834	0·622	0·332	0·427	0·384	0·505	0·495					0·232	0·101	0·016	0·204	
i3†	g, ct, chl, ta, gl, ky, ph	19·32	618·3	0·638	0·417	0·225	0·679	0·224	0·524	0·476						0·070	0·050	0·134	
i4	g, ct, cr, ta, gl, ky, ph	35·15	595·4	0·523	0·277	0·132	0·426								0·083	0·032	0·020	0·065	
i5	g, chl, bi, ta, pa, ky, ph	15·83	653·7	0·588		0·216	0·738	0·203	0·533	0·467	0·240	0·162	0·382			0·071	0·068		
i6†	ct, chl, cr, ta, pa, ky, ph	19·67	549·3		0·133	0·055	0·703	0·059	0·519	0·481					0·033	0·014	0·039		
i7†	g, ct, chl, gl, pa, ky, ph	19·01	617·8	0·647	0·427	0·232	0·686	0·231	0·525	0·475								0·139	
i8	g, chl, bi, ta, gl, pa, ph	16·61	640·5	0·633		0·239	0·701	0·229	0·525	0·475	0·265	0·122	0·430			0·079	0·058	0·145	
i9†	g, chl, ta, gl, pa, ky, ph	18·66	625·7	0·628		0·223	0·690	0·220	0·526	0·474						0·070	0·054	0·133	
i10	g, bi, ta, gl, pa, ky, ph	17·37	696·8	0·483		0·173	0·708				0·187	0·159	0·306			0·055	0·069	0·099	
i11	g, bi, ab, gl, pa, ky, ph	17·92	764·1	0·388		0·148	0·708				0·150	0·185	0·233					0·082	0·135
i12	ct, chl, cr, ta, gl, pa, ph	20·23	545·0		0·205	0·087	0·675	0·094	0·516	0·484					0·053	0·023	0·036	0·049	
i13	ct, chl, ta, gl, pa, ky, ph	19·33	603·4		0·366	0·187	0·685	0·189	0·523	0·477						0·056	0·048	0·109	
i14	ct, cr, ta, gl, pa, ky, ph	20·97	554·0		0·160	0·068	0·675								0·041	0·017	0·037	0·037	
i15	chl, bi, ta, ab, gl, pa, ph	10·80	555·3			0·037	0·725	0·036	0·510	0·490	0·055	0·108	0·117			0·011	0·040	0·022	0·737
i16	g, ct, chl, cr, gl, jd, ph	25·72	430·6	0·983	0·944	0·778	0·332	0·852	0·502	0·498					0·694			0·651	
i17†	g, ct, chl, gl, pa, jd, ph	19·32	477·8	0·986	0·959	0·852	0·549	0·889	0·508	0·492								0·763	
i18	g, ct, cr, gl, jd, ky, ph	35·02	589·1	0·579	0·322	0·155	0·435								0·099			0·078	
i19†	g, ct, gl, pa, jd, ky, ph	25·22	581·3	0·808	0·611	0·357	0·617											0·220	
i20†	g, bi, ab, pa, jd, ky, ph	21·67	802·2	0·140		0·048	0·637				0·046	0·141	0·078						0·102
i21†	g, ab, gl, pa, jd, ky, ph	21·67	802·2	0·459		0·197	0·678											0·109	0·102
i22	ct, chl, cr, ab, jd, ky, ph	14·36	507·3		0·236	0·094	0·847	0·104	0·535	0·465					0·058				0·805
i23†	ct, chl, cr, gl, pa, jd, ph	19·76	415·0		0·915	0·683	0·540	0·773	0·505	0·495					0·581			0·553	
i24†	ct, cr, gl, pa, jd, ky, ph	25·90	542·4		0·479	0·236	0·615								0·156			0·136	
i25†	g, bi, ta, ab, gl, pa, ky	16·47	748·7	0·358							0·134	0·189	0·215			0·041	0·081	0·072	0·159
i26†	g, chl, bi, ta, ab, gl, pa	13·16	658·6	0·653				0·250	0·524	0·476	0·293	0·130	0·440			0·095	0·064	0·170	0·542
i27†	g, chl, bi, ta, ab, pa, ky	11·00	685·9	0·543				0·186	0·547	0·453	0·230	0·252	0·323			0·073	0·094		0·425
i28	g, ph, bi, ab, st, pa, ky	9·13	661·6	0·804		0·448	0·874				0·477	0·393	0·294	0·817					0·503
i29	g, chl, bi, ab, st, pa, ky	8·88	658·3	0·675				0·270	0·561	0·439	0·320	0·306	0·358	0·712					0·513
i30	g, ct, ph, chl, st, pa, ky	13·85	608·4	0·777	0·595	0·359	0·800	0·356	0·546	0·454				0·787					
i31	g, ph, chl, bi, st, pa, ky	11·96	631·1	0·736		0·332	0·821	0·318	0·552	0·448	0·356	0·240	0·416	0·756					

*x(phases) = Fe/(Mg + Fe) where phases represent g, ct, ph, chl, bi, st, cr, ta and gl. The other composition variables are as in Table 1.
†The invariant points correspond to those in the petrogenetic grid of Guiraud *et al*. (1990).

Downloaded from http://petrology.oxfordjournals.org/ at Pennsylvania State University on March 5, 2016

and i27, chlorite reacts out with glaucophane and albite through reactions 25 (chl + gl = g + ta + pa) and 30 (chl + ab = g + ta + pa) at lower temperatures than reaction 1. However, at pressures lower than invariant point i27, the maximum stability of chlorite is given by reactions 1 and 2 and has nothing to do with Na phases. Similarly, at pressures below invariant point i7, the stability of chloritoid is not affected by Na phases. At pressures above i7, the Na phases such as paragonite and jadeite would lead to the disappearance of chloritoid through reactions 23 (ct + pa = g + gl + ky) and 29 (ct + jd = g + gl + ky) at lower temperatures than reactions 7 and 6. The stability of carpholite will be reduced by the presence of Na phases glaucophane, paragonite and jadeite through reactions 31–34 at pressures higher than invariant point i6, but will not be affected by Na phases at lower pressures.

COMPATIBILITY DIAGRAMS

To illustrate the changes in mineral assemblage and the compositions of coexisting minerals with respect to P–T and bulk composition, a series of calculated AFM compatibility diagrams with phengite, paragonite, quartz and H_2O in excess were drawn for a traverse from locations A to J, approximately along an 8°C/km geotherm (Fig. 4).

In Fig. 4a, the ct–cr tie-line is stable. Appropriate bulk compositions that projected between the ct–cr tie-line and chlorite solid solution give the mineral assemblages ct + cr + chl, ct + chl and cr + chl. If the bulk composition is more aluminous, kyanite will coexist with chloritoid and/or carpholite. The NKFASH subsystem reaction f11 (chl + jd = fgl + pa) gives a divariant triangle chl–gl–jd in Fe- and Na-rich compositions. At this stage, chlorite is a complete solid solution between Fe and Mg end-members. When paragonite is in excess, biotite, limited by reactions such as f20, f21, f22, f23 in NKFASH, m21, m22 in NKMASH, and 24 in NKFMASH, is not stable under the P–T condition of interest. In Fig. 4b, the NKFASH reaction f1 (chl + fct = alm) leads to the appearance of almandine-rich garnet, giving the g–ct–chl divariant triangle in Fe- and Al-rich compositions, and in Fe- and Na-rich compositions, the NKFASH reaction f12 (chl + pa = alm + jd) leads to formation of another divariant triangle g–chl–jd from the breakdown of Fe-chlorite, which, in temperature, is lower than the conjugate reaction f2 (chl + ph = alm + bi) in Fe- and K-rich rocks. As P–T increases to meet the NKFMASH reaction 19 (chl + jd = g + gl + pa), the chl–jd tie-line gives way to g–gl in Fig. 4c in Fe- and Na-rich compositions. With P–T increase to location D, the full system reaction 20 (g + chl + pa = ct + gl) results in the coexistence ct + gl, and in Mg-rich compositions, the NKMASH reactions m18 (chl + gl = ta + pa) and m3 (chl +q = mcr + ta) produce the divariant triangles chl–ta–gl and chl–ta–cr, and also result in the decomposition of Mg-chlorite. From location A to D, the ct–cr tie-line is stable and both minerals become richer in Mg as P–T increases. This tie-line is broken by reaction 9 (ct + cr = chl + ky), giving rise to the chl–ky tie-line in Fig. 4e, and the NKMASH reaction m5 (cr = ta + ky) and NKFMASH reaction 12 (cr = chl + ta + ky) result in the decomposition of carpholite and the appearance of the typical whiteschist assemblage ta–ky in Mg-rich compositions (Fig. 4e). Across the full system reaction 21 (chl + ky = ct + ta), the chl–ky tie-line gives way to ct–ta in Fig. 4f, which, as indicated by its flat slope in Fig. 3, is a good pressure indicator (Chopin & Schreyer, 1983). From location F to G, the subsystem reaction f3 (fct = alm +ky) leads to the breakdown of Fe-chloritoid and the appearance of the divariant triangle g–ct–ky in Fig. 4g, and the full system reaction 16 (chl + pa = ct + ta + gl) results in the disappearance of chlorite. In this case, the full system reactions 27 (chl + bi = g + ta + ph) and 3 (chl = g + ct + ta) not involving Na-bearing phases will not take place. Across reaction 22 (ct + ta + pa = gl + ky), the ct–ta tie-line is replaced by gl–ky in Fig. 4h, and the NKMASH reaction m12 (ta + pa = gl + ky) leads to the disappearance of Mg-talc. With P–T increase across reaction 23 (ct + pa = g + gl + ky), chloritoid breaks down and g + ky + gl can coexist in Fig. 4i. With further P–T increase across reaction n2 (pa = ky + jd), paragonite breaks down and jadeite coexists with kyanite; the phase topology shown in Fig. 4j has jadeite in excess.

For a traverse from location K to R, approximately along a 10°C/km geotherm, the changes in phase topology are shown in Fig. 5. In Fig. 5k, the chl–ky tie-line is present and carpholite is not present by virtue of the full system reaction 9 (cr + ct = chl + ky) and the subsystem reaction m4 (mcr = chl + ky) in Al- and Mg-rich compositions. The NKFASH reaction f1 (chl + fct = alm) leads to the divariant triangle g–ct–chl in Fe- and Al-rich compositions. In K-rich compositions, Mg-rich biotite is not stable by virtue of the NKMASH reactions such as m21 and m22, but Fe-rich biotite is stable. The subsystem reaction f2 (ph + chl = bi + alm) leads to the decomposition of Fe-chlorite, producing the divariant triangle g–bi–chl, reaction f8 (fgl + ph = bi + ab + pa) leads to the decomposition of Fe-glaucophane, producing the assemblage bi + gl + ab, and reaction 37 (chl + ab + ph = bi + gl + pa) results in the replacement of the chl–ab tie-line by bi–gl in Fe-, Na- and K-rich compositions. With P–T increase to location L, the chl–bi tie-line is replaced by g–gl through reaction 24 (chl + bi + pa = g + gl + ph, to

Downloaded from http://petrology.oxfordjournals.org/ at Pennsylvania State University on March 5, 2016

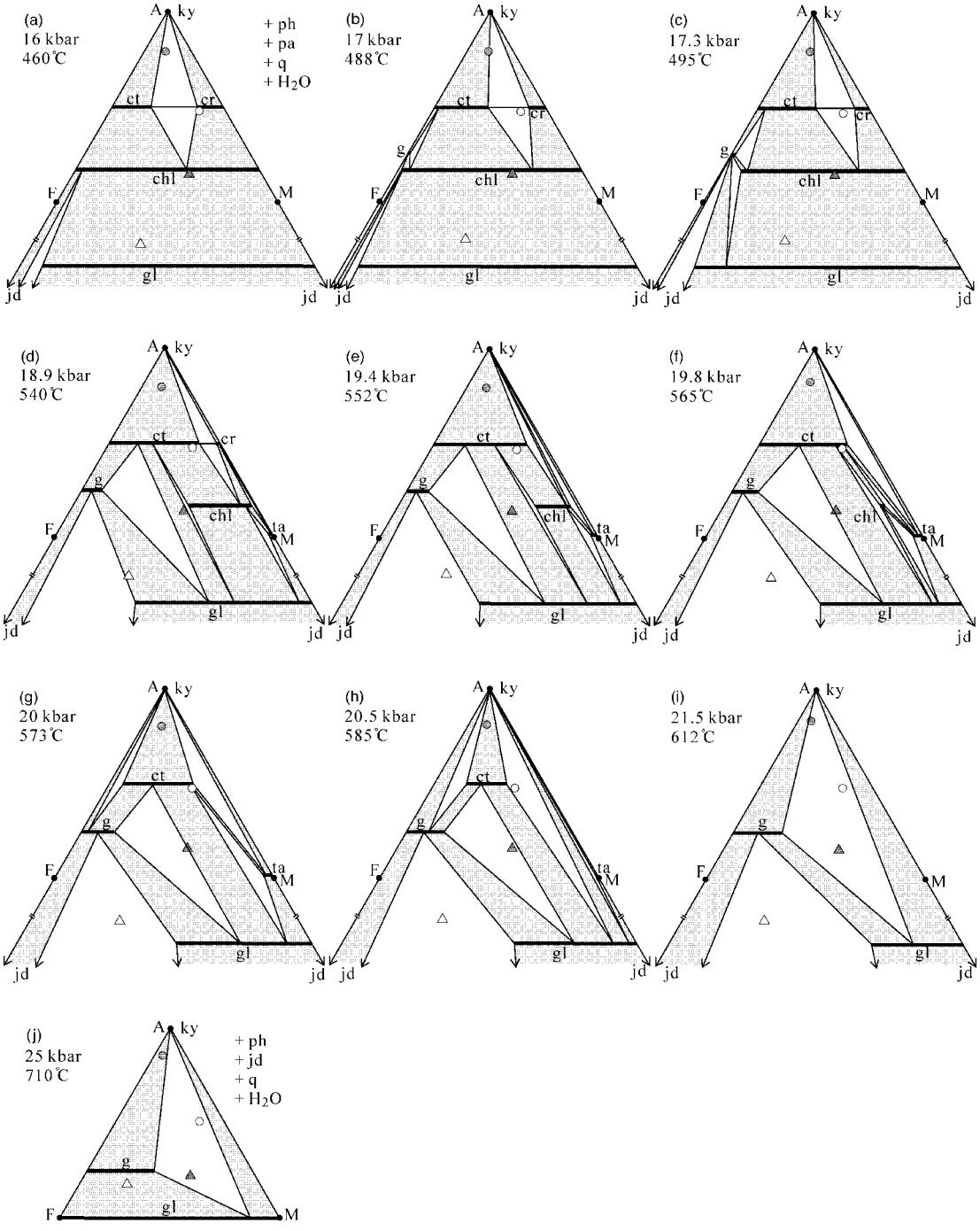

Fig. 4. AFM compatibility diagrams, in projection from phengite, quartz, H_2O and paragonite or jadeite when paragonite is out, calculated for the locations A–J labelled in Figs 1–3 and their P–T conditions. In (a)–(i), glaucophane is plotted at A = −1/3 for clarity, rather than at A = −3. Jadeite plots at A = −∞. Shaded circle, shaded triangle, open circle and open triangle represent respectively the projections of bulk composition of samples CHM1, 7-172, P80/82 and AK07 discussed in the later sections.

the left of the singularity), and Fe-biotite is broken down through reaction f23 (bi + pa = alm + ab + ph), producing the divariant assemblage g–bi–ab. In Fig. 5m, the reaction 38 (bi + pa = g + ab + gl + ph, to the left of the singularity) leads to breakdown of the surviving biotite, and reaction m18 (chl + gl = ta + pa) produces the divariant triangle chl–gl–ta in Mg- and Na-rich compositions. With P–T increase to location N, the NKFASH reaction f3 (fct = alm + ky) first results in the breakdown of Fe-chloritoid

Downloaded from http://petrology.oxfordjournals.org/ at Pennsylvania State University on March 5, 2016

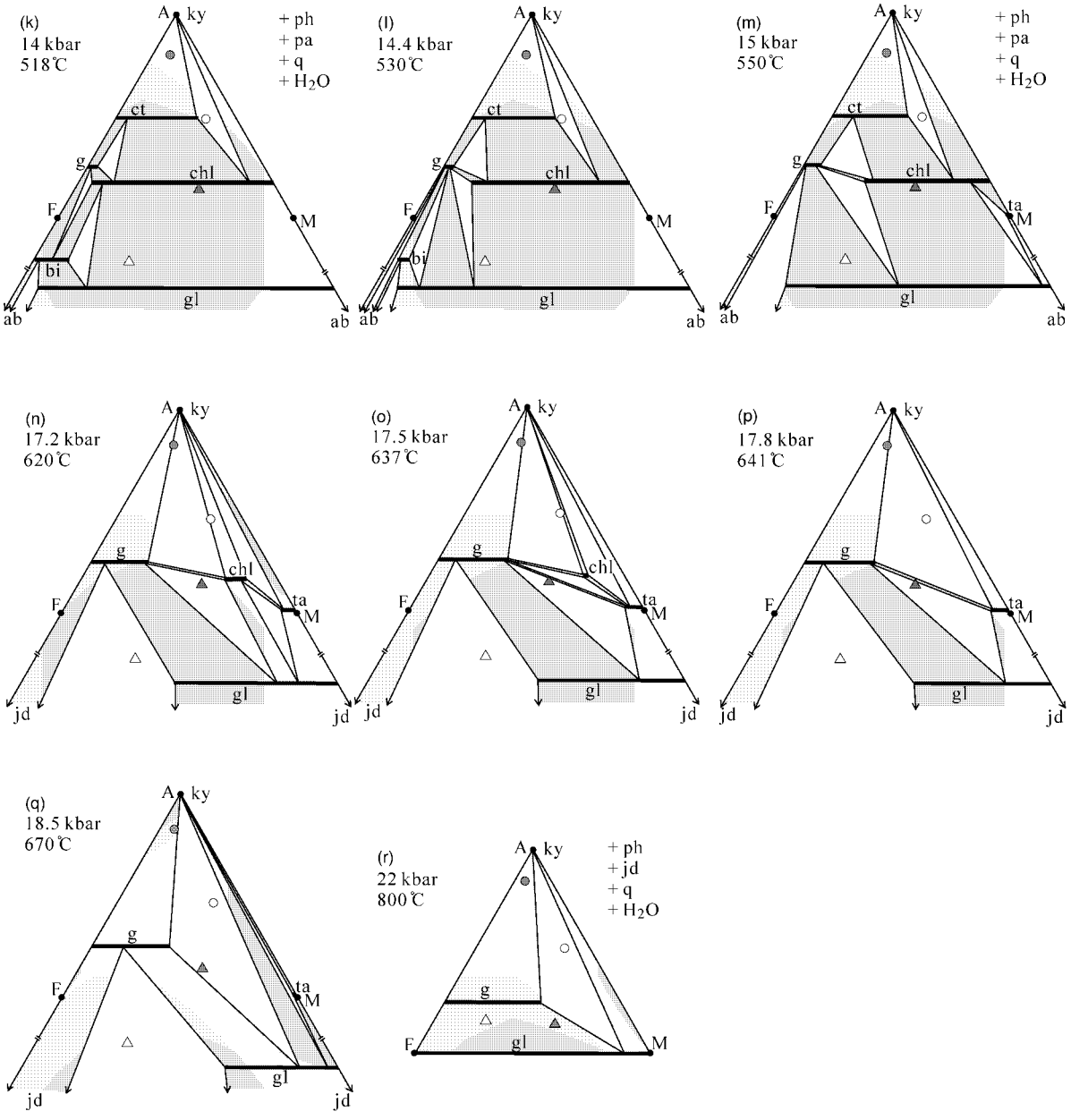

Fig. 5. AFM compatibility diagrams in projection from phengite, quartz, H_2O and paragonite or jadeite when paragonite is out, calculated for the locations K–R labelled in Figs 1–3 and their P–T conditions. (For other definitions, see Fig. 4.)

and coexistence of garnet with kyanite in Fe- and Al-rich rocks, followed by albite transformation into jadeite in Na-rich compositions; then, the NKMASH reaction m1 (chl = ta + ky) results in the disappearance of Mg-chlorite and formation of the whiteschist paragenesis ta–ky in Mg-rich compositions; finally, the NKFMASH reaction 6 (ct = g + chl + ky) leads to the breakdown of chloritoid and the paragenesis of g–chl–ky in Al-rich compositions (see Fig. 5n). From location N to O, the chl–gl tie-line gives way to g–ta through reaction 25 (chl + gl = g + ta + pa). Chlorite breaks down to produce the assemblage g + ta + ky through reaction 1 with the phase topology shown in Fig. 5p. From location P to Q, reaction 26 (g + ta + pa = gl + ky) leads to replacement of the g–ta tie-line by gl–ky (Fig. 5q). With further P–T increase, the NKMASH reaction m12 (ta + pa = gl + ky) first results in the decomposition of Mg-talc, and finally, reaction n2 leads to the breakdown of paragonite, with the phase topology shown in Fig. 5r with jadeite assumed to be in excess.

Downloaded from http://petrology.oxfordjournals.org/ at Pennsylvania State University on March 5, 2016

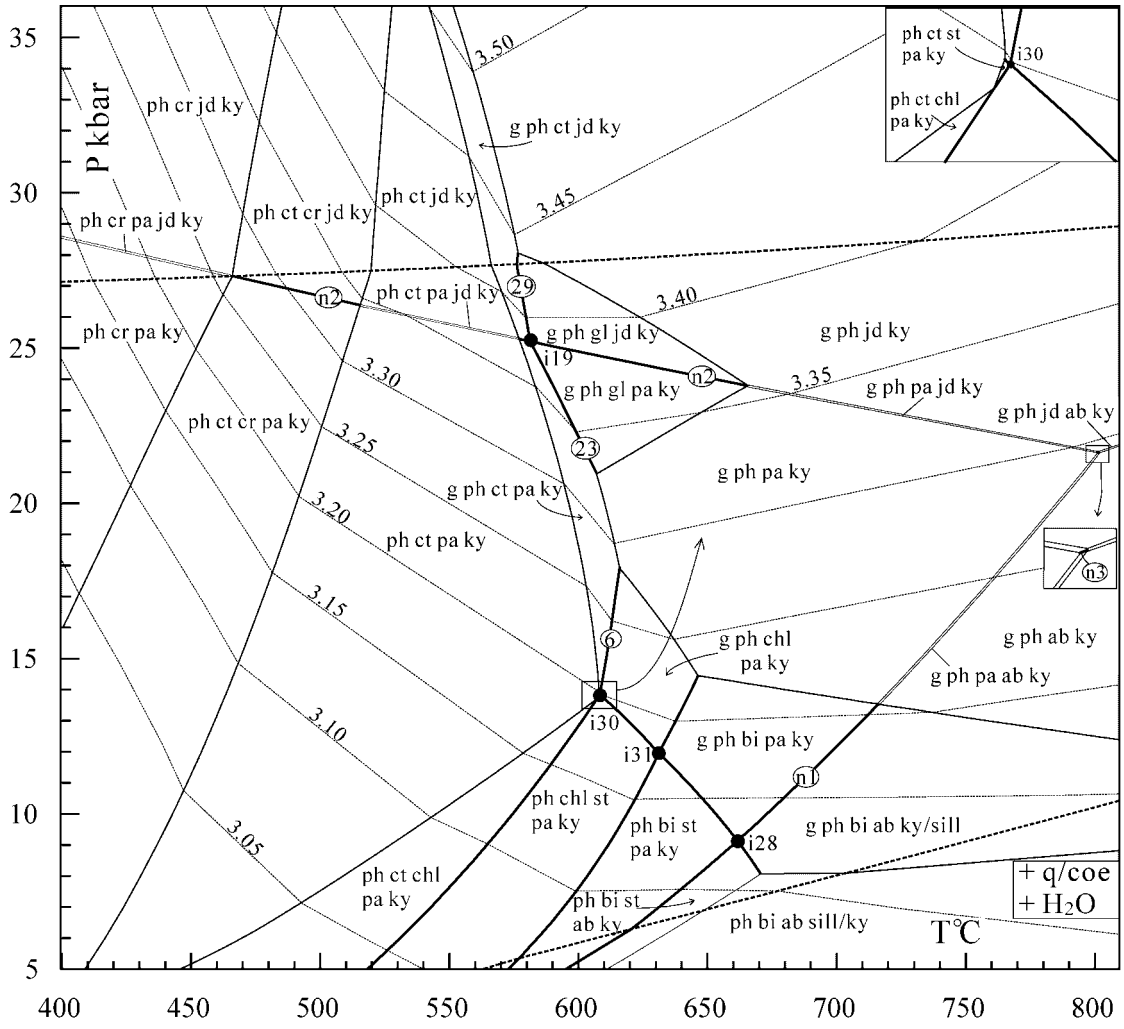

Fig. 6. *P–T* pseudosection in the NKFMASH system, with quartz and H_2O in excess, for a high-*P* metapelite (sample CHM1) from the Central Alps (Meyre *et al*., 1999) with Al_2O_3:MgO:FeO:K_2O:Na_2O = 75·65:6·53:7·85:7·89:2·08 on a mole basis, showing the invariant points (●), univariant reactions (bold continuous lines) with the labels the same as in Fig. 3, divariant fields (unshaded) and trivariant fields (light grey) encountered by the bulk composition. Isopleths of the Si content in phengite are shown as the dashed lines with numbers (Si =) 3·05–3·50 p.f.u.

Compared with the phase topologies along the geotherm of 8°C/km, there is no coexistence of chloritoid–glaucophane and chloritoid–talc, and chloritoid breaks down before chlorite for the 10°C/km geotherm.

For reference, four bulk compositions, which will be discussed in the next section, are projected on each AFM diagram in Figs 4 and 5.

APPLICATIONS

Four types of pelitic assemblages from different high *P*/*T* metamorphic terranes are selected to apply the NKFMASH grid in Fig. 3.

High-*P* metapelites from the Central Alps

Meyre *et al*. (1999) described some Tertiary high-*P* metapelites from the Adula Nappe, Central Alps, Switzerland, which are generally composed of garnet, phengite, kyanite, quartz with or without paragonite. A representative sample (CHM1) contains phengite (40%) + garnet (10%) + paragonite (10%) + kyanite (20%) + quartz (20 vol. %). Using these mineral modal proportions, together with the microprobe analyses listed by Meyre *et al*. (1999), an effective bulk composition (Vance & Holland, 1993) can be generated with the software THERMOCALC, giving Al_2O_3:MgO:FeO:K_2O:Na_2O = 75·65:6·53:7·85:7·89:2·08 on a mole basis. Using this bulk composition, a *P–T* pseudosection calculated for sample CHM1 is presented in Fig. 6. It is characterized by the prevalence of di- and trivariant fields with four invariant points seen. This pseudosection also shows the Si isopleths in phengite, which are negatively sloped at temperatures below about 600°C and positively sloped at

Downloaded from http://petrology.oxfordjournals.org/ at Pennsylvania State University on March 5, 2016

higher temperatures. The observed assemblage g + ky + pa + ph + q for sample CHM1 is trivariant in NKFMASH and stable over a P–T range with pressures about 13–24 kbar and temperatures between 600 and 800°C. The measured phengite Si content in the sample is 3·38, which would place it in the jadeite field in Fig. 6. However, the microprobe analysis for this phengite presented by Meyre *et al.* (1999) has total divalent cations (Fe^{2+} + Mg) in the M2A site of only 0·33, which should indicate the maximum celadonite content. With this, the isopleth with Si = 3·33 provides a P–T range of 21–23 kbar and 610–710°C in the trivariant field g–ph–pa–ky of Fig. 6, which is similar to the P–T conditions of 23·5–26 kbar and 620–700°C estimated for sample CHM39 in the KFMASH system (Wei & Powell, 2003), and also similar to the peak pressure condition of 25 kbar provided by Meyre *et al.* (1999) from the associated sodic whiteschist samples in the Adula Nappe.

Talc–phengite high-grade pelitic blueschists of the Western Alps

Chopin (1981) reported that the assemblage talc–phengite is widespread in the high-grade pelitic blueschist-facies rocks in and around the Gran Paradiso Massif of the western Alps. The rocks are composed essentially of talc, phengite, chloritoid and quartz (± chlorite, ± garnet, ± glaucophane). For example, one representative sample (7-172) contains g + ct + ta + chl + ph + gl + q, with a bulk composition, presented by Chopin (1981), of SiO_2 51·06, Al_2O_3 15·51, FeO 12·18, MgO 10·38, K_2O 0·46 and Na_2O 1·31 (wt %), giving Al_2O_3:MgO:FeO:K_2O:Na_2O = 25·13:42·56:28·01:0·81:3·49 on a mole basis. Using this bulk composition, a calculated P–T pseudosection is presented in Fig. 7, which is dominated by di- and trivariant fields with two quadrivariant fields and 10 invariant points that can be seen by this bulk composition. Contouring of the phengite Si isopleths for the phengite-bearing fields indicates that the Si contents rise linearly with pressure, which, however, is evidently dependent on mineral assemblage. For example, the phengite Si contents vary smoothly in most tri- and divariant fields, but trivially in the trivariant field ph–chl–gl–pa, and actually are constant in the quadrivariant field g–ph–gl. For this bulk composition, phengite is not in excess for the fields in the high-T/P part of Fig. 7 where biotite appears as a major phase, and paragonite is consumed via reactions 15, 18 and 20, etc. as a result of chlorite being in excess. Hence, the KFMASH reactions 1, 3, 4 and 7 take place to lead to the final decomposition of chlorite and chloritoid. The mineral assemblage observed in sample 7-172 is univariant in the NKFMASH system, corresponding to reaction 3 (chl + q = g + ta + ct) with glaucophane and phengite also present. The phengite in this mineral assemblage has Si = 3·45, and this isopleth crosses reaction 3 at 22·5 kbar and 565°C, giving a P–T condition for the rock in very good agreement with the P–T conditions of 21·7–23 kbar and 542–557°C estimated by Vidal *et al.* (2001) for the same sample (7-172c1) using their four-thermodynamic-component model for chlorite. In sample 7-172, the coexistence of gl + ct also indicates a metamorphic pressure over about 18–19 kbar from reaction 20 (see also Figs 3 and 4d–h). Therefore, like the ct–ta coexistence that indicates metamorphic pressures over 19 kbar (Chopin & Schreyer, 1983; Chopin & Monié, 1984; Wei & Powell, 2003), the ct–gl coexistence, stable at pressures over 18–19 kbar, is another metamorphic pressure indicator (Guiraud *et al.*, 1990).

Carpholite-bearing metapelites from the Peloponnese, Greece

Theye *et al.* (1992) described carpholite-bearing high-P metapelites from Western Crete and the Peloponnese, Greece, a representative sample (P80/82) of which contains ct + cr + chl + pa + ph + q and has a bulk composition of SiO_2 66·3, Al_2O_3 15·5, FeO 1·89, MgO 3·27, K_2O 1·70 and Na_2O 0·32 (wt %), giving Al_2O_3:MgO:FeO:K_2O:Na_2O = 53·78:28·71:9·31:6·38:1·83 on a mole basis. A P–T pseudosection is calculated using this bulk composition and is presented in Fig. 8. It is dominated by di- and trivariant fields with two quadrivariant fields and 11 invariant points that can be seen by this bulk composition. Contouring of the phengite Si isopleths for the phengite-bearing fields indicates that the Si contents rise linearly with pressure in most tri- and divariant fields, descend with pressure in the trivariant field ph–cr–pa–jd, and are constant in the two quadrivariant fields ph–cr–jd (Si = 3·20) and ph–cr–pa (Si = 3·35). The mineral assemblage observed in sample P80/82 is divariant in the NKFMASH system, forming a long narrow field with temperatures below 540°C and pressures less than 20 kbar. The Si contents of phengite in the carpholite schist are measured as 3·20, which yield a P–T condition of 14–16 kbar and 450–510°C, in the range of P–T values estimated by Theye & Seidel (1991) of 450 ± 30°C and 17 ± 4 kbar for the Peloponnese.

Glaucophane–phengite schist from the southern Tianshan high-P belt, NW China

The eclogites and blueschists in the southern Tianshan high-P belt, NW China, have been the subject of several studies recently (Gao *et al.*, 1995, 1999; Zhang *et al.*, 2002*a*, 2002*b*; Wei *et al.*, 2003). However, the

Downloaded from http://petrology.oxfordjournals.org/ at Pennsylvania State University on March 5, 2016

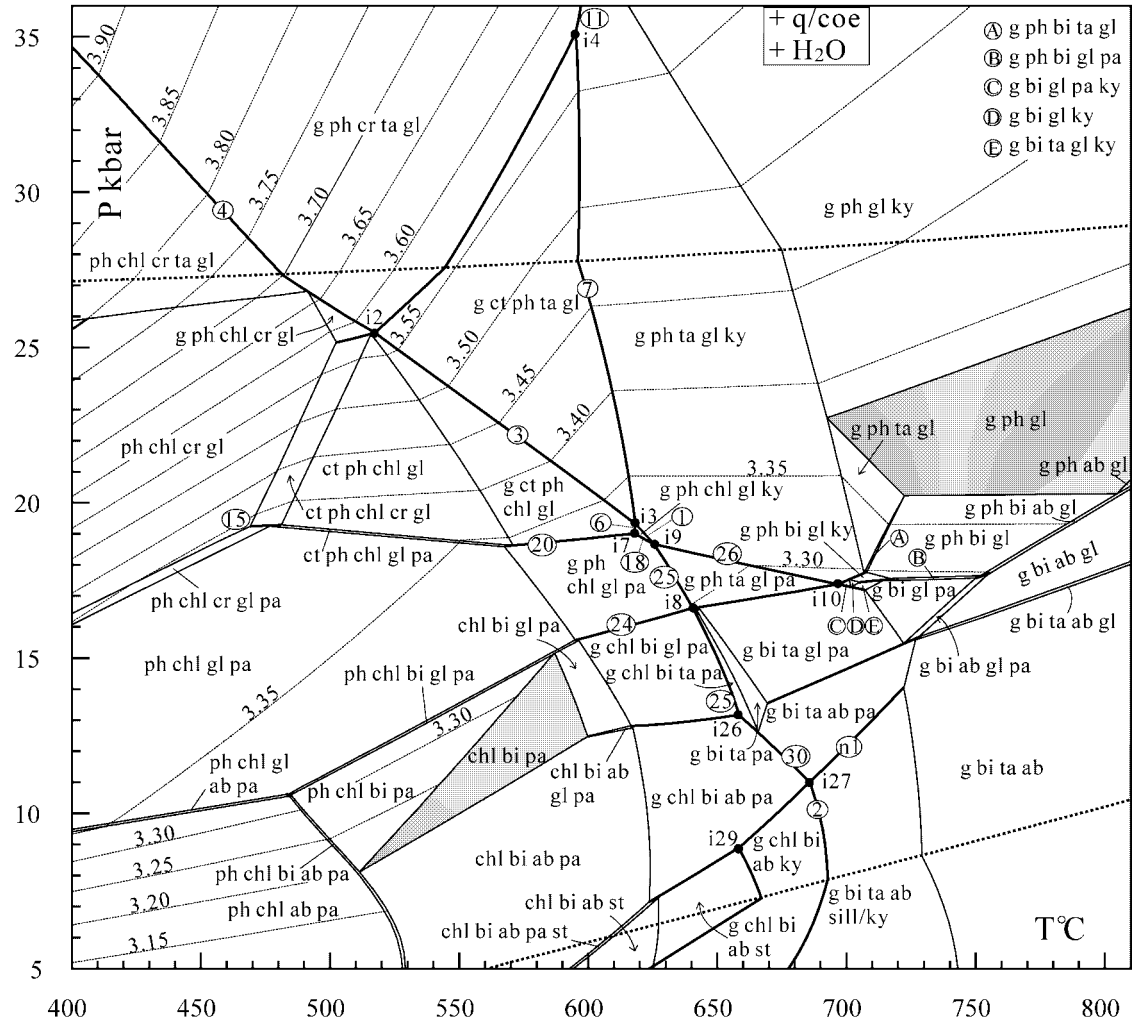

Fig. 7. *P–T* pseudosection in the NKFMASH system, with quartz and H_2O in excess, for a high-grade blueschist (sample 7-172) from the Western Alps (Chopin, 1981) with Al_2O_3:MgO:FeO:K_2O:Na_2O = 25·13:42·56:28·01:0·81:3·49 on a mole basis, showing the invariant points (●), univariant reactions (bold continuous lines) with labels the same as in Fig. 3, divariant fields (unshaded), trivariant fields (light grey) and quadrivariant fields (dark grey). Isopleths of the Si content in phengite are shown as the dashed lines with numbers (Si=) 3·15–3·90 p.f.u.

glaucophane–phengite schist, one of the most extensive rock-types in the belt, has not been well delineated, especially for its *P–T* conditions, nor for its relations with the eclogites and blueschists, because of the lack of appropriate geothermobarometers. This schist is composed mainly of garnet, phengite, glaucophane, albite, rutile, ilmenite and sphene, and probably was once a greywacke. As an example, we selected a representative sample (AK07), which contains garnet (18) + phengite (20) + glaucophane (12) + albite (35) + quartz (10 vol. %) and small amount of rutile and ilmenite. The microprobe analyses for the main minerals are garnet: SiO_2 37·83, Al_2O_3 21·01, FeO 31·97, MgO 3·00, CaO 4·91 (wt %); phengite: SiO_2 51·29, Al_2O_3 27·23, FeO 1·84, MgO 3·56, K_2O 10·48 (wt %); glaucophane: SiO_2 58·45, Al_2O_3 12·08, FeO 9·46, MgO 9·82, Na_2O 7·61 (wt %); albite: SiO_2 70·03, Al_2O_3 19·52, Na_2O 11·36 (wt %). If the small amount of CaO in the garnet is neglected, an effective bulk composition for sample AK07 can be generated in the NKFMASH system using THERMOCALC from the above mineral modal proportions and compositions, giving Al_2O_3:MgO:FeO:K_2O:Na_2O = 42·83:8·63:16·91:5·13:26·50 on a mole basis. Using this bulk composition, a *P–T* pseudosection was calculated for sample AK07 and is presented in Fig. 9. This pseudosection includes di-, tri- and quadrivariant fields with only one invariant point i23 that can be seen by this bulk composition. When compared with the previous rocks, AK07 is characterized by being Na-rich, so a prominent feature of its *P–T* pseudosection is that albite is present in every di-, tri- and quadrivariant fields below reaction n3 (jd + q = ab), as is jadeite above this reaction.

Downloaded from http://petrology.oxfordjournals.org/ at Pennsylvania State University on March 5, 2016

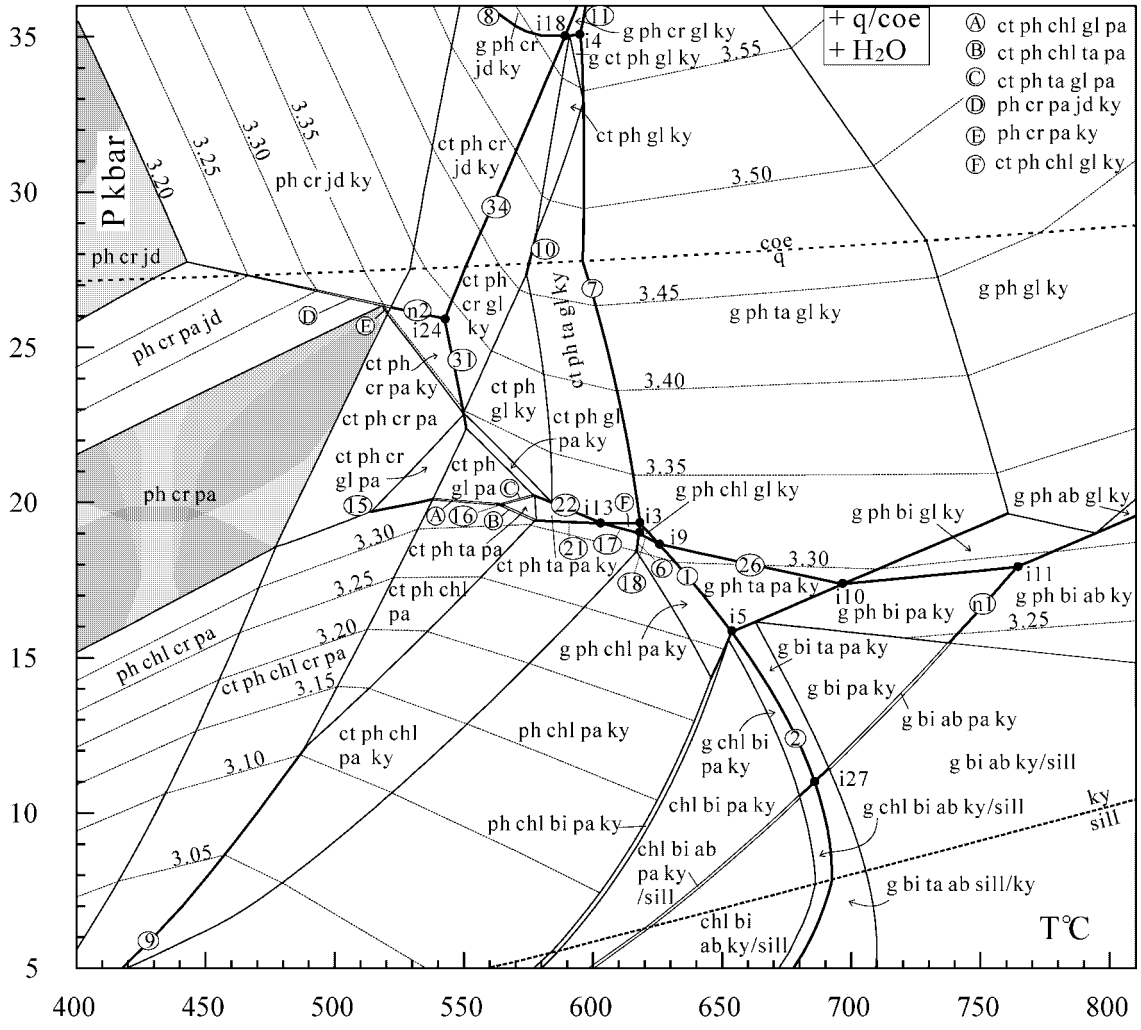

Fig. 8. *P–T* pseudosection in the NKFMASH system, with quartz and H_2O in excess, for a carpholite-bearing high-*P* metapelite (sample P80/82) from the Peloponnese, Greece, Al_2O_3:MgO:FeO:K_2O:Na_2O = 53·78:28·71:9·31:6·38:1·83 on a mole basis, showing the invariant points (●), univariant reactions (bold continuous lines) with the labels the same as in Fig. 3, divariant fields (unshaded), trivariant fields (light grey) and quadrivariant fields (dark grey). Isopleths of the Si content in phengite are shown as the dashed lines with numbers (Si=) 3·05–3·55 p.f.u.

The phengite Si isopleths are shown in this pseudosection where the Si contents rise linearly with pressure in most tri- and divariant fields, but being effectively constant in the quadrivariant field g + ph + jd (Si = 3·554), and varying irregularly in the fields in the central-left part of Fig. 9. For example, the Si isopleths are steeply and negatively sloped in the divariant field g–ph–gl–pa–jd, descending trivially with temperature, and in the trivariant field g–ph–gl–ab, the Si isopleths are moderately and positively sloped, rising clearly with temperature. The observed mineral assemblage for sample AK07 is trivariant in the NKFMASH system and takes up a small irregular triangle just adjacent to reaction n3. The measured Si content in phengite is 3·40, giving a *P–T* condition of about 17–19 kbar and 670–690°C in Fig. 9, where the pressure is in good agreement with that of a hornblende eclogite in the belt estimated at 17–18 kbar, with temperature being slightly higher than that estimated there, 610–630° (Wei *et al.*, 2003). With reference to the temperature estimates for the eclogites from the southern Tianshan of 480–580°C (Gao *et al.*, 1999) and 500–600°C (Zhang *et al.*, 2002*a*) based on the garnet–clinopyroxene geothermometer, the temperature 670–690°C for the glaucophane–phengite schist is probably a small overestimate. One of the probable reasons for this is that the CaO in garnet affected the temperature estimation. As a result, the hornblende eclogites are coherent with their surrounding rocks at least in metamorphic conditions.

Downloaded from http://petrology.oxfordjournals.org/ at Pennsylvania State University on March 5, 2016

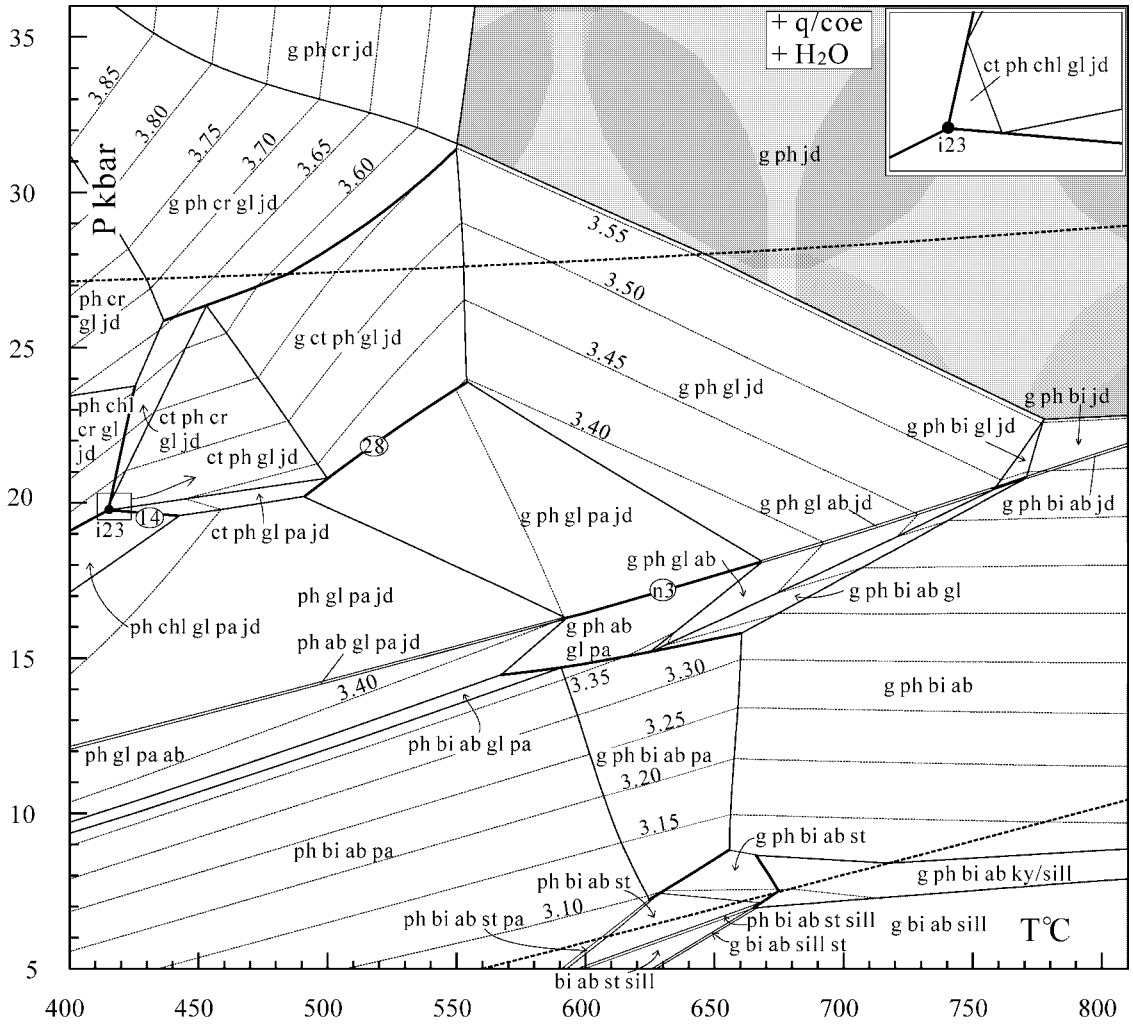

Fig. 9. *P–T* pseudosection in the NKFMASH system, with quartz and H_2O in excess, for a glaucophane–phengite schist (sample AK07) from the Southern Tianshan, NW China with Al_2O_3:MgO:FeO:K_2O:Na_2O = 42·83:8·63:16·91:5·13:26·50 on a mole basis, showing the invariant points (●), univariant reactions (bold continuous lines) with the labels the same as in Fig. 3, divariant fields (unshaded), trivariant fields (light grey) and quadrivariant fields (dark grey). Isopleths of the Si content in phengite are shown as the dashed lines with numbers (Si=) 3·10–3·85 p.f.u.

DISCUSSION AND CONCLUSION

Comparison with published petrogenetic grids

Guiraud *et al.* (1990) calculated an NFMASH grid for the greenschist–blueschist–eclogite facies in the range 5–50 kbar and 300–850°C. Of the 18 invariant points presented in their grid, there are 13 corresponding to the invariant points with an asterisk in Table 3 but with distinctively different *P–T* conditions because of differences in the internally consistent dataset and the different models of activity–composition relationships for the solid solutions used, which, in turn, leads to considerable differences in the phase topologies between the two grids. Of these differences, a few are notable, as follows.

(1) For pressures above invariant i3, the chlorite-out reaction 3 in Fig. 3 shows a moderately negative slope, which, to some extent, can be used as a pressure indicator; whereas in the grid of Guiraud *et al.* (1990), the corresponding reaction is steeply sloped, being a good temperature indicator.

(2) According to the grid of Guiraud *et al.* (1990), garnet and carpholite occur together under extremely high pressures ($P > 44$ kbar, $T < 600$°C). In contrast, the present study suggests that the garnet–carpholite paragenesis can occur if pressures are greater than only 25 kbar and temperatures lower than 550–600°C, which would be attainable in nature.

(3) The involvement of K_2O and relevant phases phengite and biotite in our study provides more constraints on the relatively high T/P part of the grid, for

Downloaded from http://petrology.oxfordjournals.org/ at Pennsylvania State University on March 5, 2016

instance, the invariant points i1, i5, i8, i10 and i11, as well as the reactions emanating from them (see Fig. 3). In particular, the involvement of phengite, one of the most ubiquitous phases in high-P metapelites, provides a possibility to contour relevant P–T pseudosections for its Si content, which can be used as a good geobarometer for various high-P assemblages.

High-P assemblages in Na-bearing metapelites

For decades, the unusual assemblages kyanite–talc and phengite–talc have been emphasized as high-P indicators for pelitic compositions (e.g. Abraham & Schreyer, 1976; Schreyer, 1977, 1988; Chopin, 1981; Massonne & Schreyer, 1989; Izadyar *et al.*, 2000). These assemblages are restricted to unusual pelitic compositions rich in Mg that can be modelled in the MASH and KMASH systems. Wei & Powell (2003) suggested that incorporation of Fe into the KMASH system would stabilize chloritoid and garnet, which could coexist with talc, phengite, kyanite, chlorite, carpholite and biotite, and lead to various mineral assemblages for different bulk compositions and P–T conditions. As has been demonstrated above, the incorporation of Na into the KFMASH system, with the Na phases albite, paragonite, glaucophane and jadeite considered, leads to much more complicated phase relations and diverse mineral assemblages in the NKFMASH system. It should be noted, however, that the KFMASH phase topology provides a 'backbone' for the NKFMASH phase relations. If the Na–K substitution in phengite is taken into account using Coggon & Holland (2002), the invariant equilibria containing both phengite and biotite are affected by 1–3°C in T and less than 0·5 kbar in P.

If the bulk compositions are rich in Al and poor in Mg with lesser Na, as in sample CHM1 (see its projection on the AFM diagrams of Figs 4 and 5), kyanite will be ubiquitous and coexist with carpholite, chloritoid and garnet, respectively, with increasing P–T along geotherms of 8–10°C/km. Talc would be absent, and paragonite will be stable to its maximum stability limits, giving way to jd + ky via reaction n2, and ab + ky via reaction n1, respectively. In most fields only one Na phase is present. For example, the mineral assemblage g + ct + ky + ph + pa + q reported by Vuichard & Ballèvre (1988) in an eclogitic mica-schist from the Sesia zone, Western Alps, may represent a rock with a similar composition to CHM1, but which was metamorphosed at a lower temperature, 570–600°C, limited by the subsystem reaction f3 (see Figs 2 and 4h), and the full system reaction 6, concordant with the temperature of 550–600°C estimated by Vuichard & Ballèvre (1988) using the garnet–phengite pair.

For bulk compositions rich in Mg and poor in Al with lesser Na, such as sample 7-172, the AFM phases such as chlorite and chloritoid will be stable to their maximum stability limits (see Fig. 7), talc is stable in considerably wider P–T ranges, and carpholite confined only to high P/T fields. There would be a wide P–T range for glaucophane stability, but no field for the stability of jadeite. Rocks with this composition tend to develop ct + gl (see Figs 4d–h and 7) when metamorphic pressures are above 18–19 kbar (reactions 15 and 20 in Fig. 3). This ct–gl pair would coexist with other AFM phases such as carpholite, chlorite, garnet, talc and kyanite with changes of temperature (see Figs 3 and 7) or of Fe/Mg ratio (see Fig. 4d–h), or coexist with other Na phases paragonite and jadeite if there is sufficient Na_2O in the bulk composition. This ct–gl pair has been reported in a number of regions, for example, in Ile de Groix (Kiénast & Triboulet, 1972), in Gran Paradiso, Western Alps (Chopin, 1981), in Spitsbergen (Ohta *et al.*, 1986), in Oman (El-Shazly & Liou, 1991) and in Chinese Tianshan (L. F. Zhang, personal communication, 2002). According to the thermodynamic calculations carried out in this paper and also in that of Guiraud *et al.* (1990), the ct–gl pair is a high-pressure indicator that is stable in the stability field of jadeite + quartz, although its stability field, as has been demonstrated by Guiraud *et al.* (1990), will expand with rising $X_{Fe^{3+}}$ for both glaucophane and chloritoid. The mineral assemblages g + chl + pa + gl + ph + q and g + chl + pa + ct + ph + q observed in New Caledonia by Yokoyama *et al.* (1986) and Ghent *et al.* (1987), in Alaska by Brown & Forbes (1986), in the Vendée by Guiraud *et al.* (1987), and in Sesia, Western Alps, by Vuichard & Ballèvre (1988) may represent rocks with a similar bulk composition to sample 7-172 but metamorphic pressures lower than reaction 20 (see Figs 3 and 5k,l). Their metamorphic temperatures should be above the NKFASH reaction f1 in Fig. 2 from the presence of garnet in these assemblages, but lower than reaction 25 in Fig. 3 from the chlorite–glaucophane coexistence in the former, and lower than reactions 5 and 6 from the presence of chloritoid in the latter. These P–T ranges are in agreement with the estimates from petrological studies.

For bulk compositions rich in Mg, with moderate amounts of Al and lower Na, similar to sample P80/82 (see its projection on each AFM diagram in Figs 4 and 5), carpholite will be ubiquitous at low T (below reactions 9 and 10 in Figs 3 and 8), and chlorite, talc and kyanite take its place at higher T or higher P. It is interesting that the four Na phases paragonite, albite, glaucophane and jadeite are stable, respectively, at low P–T, low P/T, high P/T and high P–T fields in Fig. 8, with limited fields where they coexist. The mineral assemblage ky + ct + chl + pa + ph + q in

Downloaded from http://petrology.oxfordjournals.org/ at Pennsylvania State University on March 5, 2016

kyanite–chloritoid mica schist described by Chen (1995) and Will *et al.* (1998) from eastern Samos, Greece, indicates a rock with similar composition to sample P80/82 but metamorphic temperature above reaction 9. The phengite in the mica schist contains Si = 3·12, yielding a metamorphic pressure of about 12·5 kbar in Fig. 8 for a temperature of 500°C estimated by Will *et al.* (1998), which is similar to that estimated by Chen (1995) and Will *et al.* (1998).

For bulk compositions rich in Na and Fe, poor in Mg and Al with moderate K, analogues to sample AK07, there will be a wide P–T range for the stability of garnet and biotite but the other AFM phases such as chlorite, chloritoid and carpholite will be stable only at high P/T. There are much wider P–T ranges for the Na phases albite, jadeite and glaucophane as well as paragonite. These Na-rich rocks would be extensive in high-P terranes around the world, but most of them, like sample AK07 in Chinese Tianshan, occur in the albite stability field. Koons (1986) reported a mineral assemblage g + gl + jd + pa + ph + q in quartzofeldspathic rocks from the Sesia Zone, Western Alps; it probably represents a rock rich in Na but metamorphic pressures are above reaction n3. This assemblage is constrained by reactions 28, 19, n2 and n3 in Fig. 3 and would be the most common assemblage for Na- and Fe-rich compositions in high-P metamorphism with geotherms along 8–10°C/km (e.g. Figs 4d–i and 5l–o). There is also a stability field for this assemblage in the central part of Fig. 9. Koons (1986) estimated a P–T condition of 600–620°C and 17·5–18·5 kbar for this quartzofeldspathic rock and measured the phengite Si content at about 3·40. This is in good agreement with the calculations in Fig. 9, with in fact Si = 3·40. Moreover, the particularly sodic metapelite from NW Turkey described by Okay (2002), with the mineral assemblage jd + ct + gl + chl + ph + q + lawsonite (samples 4892B and 4893B), is also an Fe- and Na-rich rock but represents lower T/P conditions. Excluding the only Ca-bearing phase lawsonite, the other six NKFMASH phases constitute a divariant assemblage whose P–T conditions are limited by reactions 14, 35 and 36 in Fig. 3, giving a range of 20–25 kbar and 420–480°C, similar to the pressures of 24 ± 3 kbar and temperatures of 430 ± 30°C estimated by Okay (2002).

In addition, Izadyar *et al.* (2000) reported a mineral assemblage ta + ph + ab + chl + q ± gl (crossite) in the piemontite–quartz schists from the Sanbagawa belt, Japan, which is derived from an extreme bulk composition with $Mg/(Mg + Fe^{2+})$ about 1·0. Using the thermodynamic database of Holland & Powell (1998), Izadyar *et al.* (2000) calculated a possible petrogenetic grid in the NKMASH system, in which the talc–phengite stability field was limited around 580–600°C and 11·6–12·0 kbar. As discussed by those workers, the pressure is concordant with the inferred pressures of the higher-grade part of Sanbagawa belt (Banno & Sakai, 1989), but the temperature range is unrealistically narrow to explain the occurrence of the talc–phengite assemblage from the higher garnet and biotite zones in the Sanbagawa belt, which cover the temperature range from ~500 to 630°C. The possible reason for this is that the activity–composition models for the solid solutions involved in their calculation are not reliable. According to our calculated NKMASH grid presented in Fig. 1, which is also based on the database of Holland & Powell (1998), but using updated and more reliable activity–composition models for solid solutions (for details see the Appendix), the talc–phengite stability field is limited by reactions m17 and m10 on the low-P side, covering a much wider P–T range, but the observed assemblage ta + ph + ab + chl + q ± gl takes up a small P–T range with P = 9·5–10·5 kbar and T = 490–580°C, limited by reactions m17 (chl + bi = ta + ph), m19 (chl + ab = gl + pa) and m20 (chl + ab = ta + pa) on the consideration that albite coexists with chlorite and there is no paragonite present in this mineral assemblage. The inferred P–T condition is in good agreement with the petrological studies of Banno & Sakai (1989).

Accordingly, the calculated P–T grids presented in Figs 1–3 are powerful in delineating the phase relations for Na-bearing metapelites from high-P terranes around the world. If combined with the calculated P–T pseudosection for the bulk composition of a mineral assemblage of interest, contoured for isopleths of mineral compositions, e.g. the Si content of phengite, more accurate information on the P–T conditions and evolution can be derived.

Phengite geobarometry in the NKFMASH system

According to the experimental calibrations of the phengite Si contents in limited KMASH assemblages (Massonne & Schreyer, 1987, 1989; Massonne & Szpurka, 1997), phengite shows a high potential for geobarometry. This has been supported by the calculated results in the KMASH and KFMASH systems in a previous paper (Wei & Powell, 2003). In the NKFMASH system, the phengite geobarometry, as shown in Figs 6–9, varies with mineral assemblage, or more precisely, with how many Na phases are involved in the mineral assemblage. If there is only one Na phase present in the mineral assemblage, the NKFMASH phengite at fixed P–T conditions has a lower Si content and identical slope of the Si isopleths when compared with the similar mineral assemblage in the KFMASH system. For example, at P = 20 kbar

Downloaded from http://petrology.oxfordjournals.org/ at Pennsylvania State University on March 5, 2016

and $T = 671°C$, the NKFMASH phengite in a trivariant assemblage coexisting with garnet, paragonite, kyanite and quartz has Si = 3·30 from Fig. 6, and the KFMASH phengite in a similar trivariant assemblage free of paragonite has Si = 3·32 from fig. 8 of Wei & Powell (2003), with the KFMASH phengite decreasing its Si content at fixed P and T as paragonite is incorporated. Similarly, at $P = 20$ kbar and $T = 471°C$, the NKMASH phengite in a trivariant assemblage with chlorite, carpholite, glaucophane and quartz has Si = 3·42 in Fig. 7, and the KFMASH phengite in a similar trivariant assemblage without glaucophane has Si= 3·45 from fig. 6 of Wei & Powell (2003). However, when there are two or more Na-bearing phases present in the mineral assemblage, the phengite Si isopleths show much more complicated relationships with P–T conditions. As shown in Fig. 9, the phengite Si isopleths are gently and positively sloped and smoothly rise with pressure in the trivariant assemblage ph–bi–ab–pa and divariant assemblage g–ph–bi–ab–pa, whereas in the divariant assemblage g–ph–gl–pa–jd, the phengite Si isopleths are steeply and negatively sloped, gently decreasing with temperature. In this case, phengite can not be used as a geobarometer. Therefore care must be exercised in using phengite Si as a geobarometer.

ACKNOWLEDGEMENTS

This work was financially supported by the National Natural Science Foundation of China (Grant number 40172031) and undertaken while C.J.W. was a visitor in the School of Earth Sciences at the University of Melbourne. R.P. thanks the Australian Research Council for continuing support. We are grateful to Christian Chopin, Michel Guiraud and Frank Spear for constructive reviews of the manuscript. Professor Kurt Bucher is thanked for his careful editorial work.

REFERENCES

Abraham, K. & Schreyer, W. (1976). A talc–phengite assemblage in piemontite schist from Brezovica, Serbia, Yugoslavia. *Journal of Petrology* **17**, 421–439.

Banno, S. & Sakai, C. (1989). Geology and metamorphic evolution of the Sanbagawa metamorphic belt, Japan. In: Daly, J. S., Cliff, R. A. & Yardley, B. W. D. (eds) *Evolution of Metamorphic Belts. Geological Society, London, Special Publications* **43**, 519–532.

Brown, E. H. & Forbes, R. B. (1986). Phase petrology of eclogitic rocks in the Fairbanks district, Alaska. *Geological Society of America, Memoirs* **164**, 155–167.

Chen, G. (1995). Evolution of the high- and medium-pressure metamorphic rocks on the island of Samos, Greece. *Annales Géologiques des Pays Helléniques (1)* **36**, 799–915.

Chopin, C. (1981). Talc–phengite: a widespread assemblage in high-grade pelitic blueschists of the western Alps. *Journal of Petrology* **22**, 628–650.

Chopin, C. & Monié, P. (1984). A unique magnesiochloritoid-bearing, high-pressure assemblage from the Monte Rosa, Western Alps: petrologic and $^{40}Ar/^{39}Ar$ radiometric study. *Contributions to Mineralogy and Petrology* **87**, 388–398.

Chopin, C. & Schreyer, W. (1983). Magnesiocarphollite and magnesiochloritoid: two index minerals of pelitic blueschists and their preliminary phase relations in the model system $MgO–Al_2O_3–SiO_2–H_2O$. *American Journal of Science* **283-A** Orville volume, 72–96.

Coggon, R. & Holland, T. J. B. (2002). Mixing properties of phengitic micas and revised garnet–phengite thermobarometers. *Journal of Metamorphic Geology* **20**, 683–696.

Dale, J., Holland, T. & Powell, R. (2000). Hornblende–garnet–plagioclase thermobarometry: a natural assemblage calibration of the thermodynamics of hornblende. *Contributions to Mineralogy and Petrology* **140**, 353–362.

El-Shazly, A. K. & Liou, J. G. (1991). Glaucophane chloritoid-bearing assemblages from NE Oman: petrologic significance and a petrogenetic grid for high-P metapelites. *Contributions to Mineralogy and Petrology* **107**, 180–201.

Gao, J., He, G., Li, M., Xiao, X., Tang, Y., Zhou, M. & Wang, J. (1995). The mineralogy, petrology, metamorphic PTDt trajectory and exhumation mechanism of blueschists, south Tianshan, northwestern China. *Tectonophysics* **250**, 151–168.

Gao, J., Klemd, R., Zhang, L., Wang, Z. & Xiao, X. (1999). P–T path of high-pressure/low-temperature rocks and tectonic implications in the western Tianshan Mountains, NW China. *Journal of Metamorphic Geology* **17**, 621–636.

Ghent, E. D., Stout, M. Z., Black, P. M. & Brothers, R. N. (1987). Chloritoid-bearing rocks associated with blueschists and eclogites, northern New Caledonia. *Journal of Metamorphic Geology* **5**, 239–254.

Guiraud, M., Burg, J. P. & Powell, R. (1987). Evidence for a Variscan suture zone in the Vendée, France: a petrological study of blueschist facies rocks from Bois de Cene. *Journal of Metamorphic Geology* **5**, 225–237.

Guiraud, M., Holland, T. J. B. & Powell, R. (1990). Calculated mineral equilibria in the greenschist–blueschist–eclogite facies in $Na_2O–FeO–MgO–Al_2O_3–SiO_2–H_2O$: methods, results and geological applications. *Contributions to Mineralogy and Petrology* **104**, 85–98.

Holland, T. J. B. (1988). Preliminary phase relations involving glaucophane and applications to high pressure petrology: new heat capacity and thermodynamic data. *Contributions to Mineralogy and Petrology* **99**, 134–142.

Holland, T. J. B. & Powell, R. (1990). An enlarged and updated internally consistent thermodynamic dataset with uncertainties and correlations: the system $K_2O–Na_2O–CaO–MgO–MnO–FeO–Fe_2O_3–Al_2O_3–TiO_2–SiO_2–C–H_2–O_2$. *Journal of Metamorphic Geology* **8**, 89–124.

Holland, T. & Powell, R. (1996). Thermodynamics of order–disorder in minerals: I. Symmetric formalism applied to minerals of fixed composition. *American Mineralogist* **81**, 1413–1424.

Holland, T. J. B. & Powell, R. (1998). An internally consistent thermodynamic data set for phases of petrological interest. *Journal of Metamorphic Geology* **16**, 309–343.

Holland, T., Barker, J. & Powell, R. (1998). Mixing properties and activity–composition relationships of chlorites in the system $MgO–FeO–Al_2O_3–SiO_2–H_2O$. *European Journal of Mineralogy* **10**, 395–406.

Izadyar, J., Hirajima, T. & Nakamura, D. (2000). Talc–phengite–albite assemblage in piemontite–quartz schist of the Sanbagawa

Downloaded from http://petrology.oxfordjournals.org/ at Pennsylvania State University on March 5, 2016

metamorphic belt, central Shikoku, Japan. *Island Arc* **9**, 145–158.

Kiénast, J. R. & Triboulet, C. (1972). Le chloritoïde dans les paragenèses à glaucophane, albite ou paragonite. *Bulletin de la Société Française de Minéralogie et de Cristallographie* **95**, 565–573.

Koons, P. O. (1986). Relative geobarometry from high-pressure rocks of quartzofeldspathic composition from the Sesia–Lanzo Zone, Western Alps, Italy. *Contributions to Mineralogy and Petrology* **93**, 322–334.

Massonne, H. J. & Schreyer, W. (1987). Phengite geobarometry based on the limiting assemblages with K-feldspar, phlogopite and quartz. *Contributions to Mineralogy and Petrology* **96**, 212–224.

Massonne, H. J. & Schreyer, W. (1989). Stability field of the high-pressure assemblage talc–phengite and two new phengite barometers. *European Journal of Mineralogy* **1**, 391–410.

Massonne, H. J. & Szpurka, Z. (1997). Thermodynamic properties of white micas on the basis of high-pressure experiments in the systems K_2O–MgO–Al_2O_3–SiO_2–H_2O and K_2O–FeO–Al_2O_3–SiO_2–H_2O. *Lithos* **41**, 229–250.

Meyre, C., Capitani, C., Zack, T. & Frey, M. (1999). Petrology of high-pressure metapelites from the Adula Nappe (Central Alps, Switzerland). *Journal of Petrology* **40**, 199–213.

Ohta, Y., Hirijima, T. & Hiroi, Y. (1986). Caledonian high-pressure metamorphism in Central Western Spitsbergen. *Geological Society of America, Memoirs* **164**, 205–216.

Okay, A. I. (2002). Jadeite–chloritoid–glaucophane–lawsonite blueschists in northwestern Turkey: unusually high P/T ratios in continental crust. *Journal of Metamorphic Geology* **20**, 757–768.

Powell, R. (1987). Darken's quadratic formalism and the thermodynamics of minerals. *American Mineralogist* **72**, 1–11.

Powell, R. & Holland, T. J. B. (1990). Calculated mineral equilibria in the pelitic system. KFMASH (K_2O–FeO–MgO–Al_2O_3–SiO_2–H_2O). *American Mineralogist* **75**, 367–380.

Powell, R. & Holland, T. J. B. (1999). Relating formulations of the thermodynamics of mineral solid solutions: activity modeling of pyroxenes, amphiboles, and micas. *American Mineralogist* **84**, 1–14.

Powell, R., Holland, T. & Worley, B. (1998). Calculating phase diagram involving solid solutions via non-linear equations, with examples using THERMOCALC. *Journal of Metamorphic Geology* **16**, 577–586.

Schreyer, W. (1973). Whiteschist: a high-pressure rock and its geologic significance. *Journal of Geology* **81**, 735–739.

Schreyer, W. (1977). Whiteschists: their compositions and pressure temperature regimes based on experimental, field and petrographic evidence. *Tectonophysics* **34**, 127–144.

Schreyer, W. (1988). Experimental studies on metamorphism of crustal rocks under mantle pressures. *Mineralogical Magazine* **52**, 1–26.

Theye, T. & Seidel, E. (1991). Petrology of low-grade high-pressure metapelites from the External Hellenides (Crete, Peloponnese). A case study with attention to sodic minerals. *European Journal of Mineralogy* **3**, 343–366.

Theye, T., Seidel, E. & Vidal, O. (1992). Carpholite, sudoite and chloritoid in low-grade high-pressure metapelites from Crete and the Peloponnese, Greece. *European Journal of Mineralogy* **4**, 487–507.

Vance, D. & Holland, T. J. B. (1993). A detailed isotopic and petrological study of a single garnet from the Gassetts Schist, Vermont. *Contributions to Mineralogy and Petrology* **114**, 101–118.

Vidal, O., Parra, T. & Trotet, F. (2001). A thermodynamic model for Fe–Mg aluminous chlorite using data from phase equilibrium experiments and natural pelitic assemblages in the 100° to 600°C, 1 to 25 kb range. *American Journal of Science* **301**, 557–592.

Vuichard, J. P. & Ballèvre, M. (1988). Garnet chloritoid equilibria in eclogitic pelitic rocks from the Sesia zone (Western Alps): their bearing on phase relations in high pressure metapelites. *Journal of Metamorphic Geology* **6**, 135–157.

Wei, C. J. & Powell, R. (2003). Phase relations in high-pressure metapelites in the system KFMASH (K_2O–FeO–MgO–Al_2O_3–SiO_2–H_2O) with application to natural rocks. *Contributions to Mineralogy and Petrology* **145**, 301–315.

Wei, C. J., Powell, R. & Zhang, L. F. (2003). Eclogites from the south Tianshan, NW China: petrological characteristic and calculated mineral equilibria in the Na_2O–CaO–FeO–MgO–Al_2O_3–SiO_2–H_2O system. *Journal of Metamorphic Geology* **21**, 163–180.

White, R. W., Powell, R. & Holland, T. J. B. (2001). Calculation of partial melting equilibria in the system Na_2O–CaO–K_2O–FeO–MgO–Al_2O_3–SiO_2–H_2O (NCKFMASH). *Journal of Metamorphic Geology* **19**, 139–153.

Will, T., Okrusch, M., Schmädicke, E. & Chen, G. (1998). Phase relations in the greenschist–blueschist–amphibolite–eclogite facies in the system Na_2O–CaO–FeO–MgO–Al_2O_3–SiO_2–H_2O (NCFMASH), with application to metamorphic rocks from Samos, Greece. *Contributions to Mineralogy and Petrology* **132**, 85–102.

Xu, G., Will, T. M. & Powell, R. (1994). A calculated petrogenetic grid for the system K_2O–FeO–MgO–Al_2O_3–SiO_2–H_2O, with particular reference to contact-metamorphosed pelites. *Journal of Metamorphic Geology* **12**, 99–119.

Yokoyama, K., Brothers, R. N. & Black, P. M. (1986). Regional eclogite facies in the high-pressure metamorphic belt of New Caledonia. *Geological Society of America, Memoirs* **164**, 407–423.

Zhang, L. F., Ellis, D. J. & Jiang, W. B. (2002*a*). Ultrahigh-pressure metamorphism in western Tianshan, China, Part I: evidence from inclusions of coesite pseudomorphs in garnet and from quartz exsolution lamellae in omphacite in eclogites. *American Mineralogist* **87**, 853–860.

Zhang, L. F., Ellis, D. J., Williams, S. & Jiang, W. B. (2002*b*). Ultrahigh-pressure metamorphism in western Tianshan, China, Part II: evidence from magnesite in eclogite. *American Mineralogist* **87**, 861–866.

APPENDIX: MIXING MODELS, AND MINERAL AND END-MEMBER FORMULAE

Garnet (g): $[Mg,Fe]_3Al_2Si_3O_{12}$

A symmetric solution model is used for Mg–Fe mixing in binary garnet with the interaction parameter W(py, alm) = 2·5 kJ/mol following Dale *et al.* (2000). End-members:

pyrope (py), $Mg_3Al_2Si_3O_{12}$;
almandine (alm), $Fe_3Al_2Si_3O_{12}$.

Chloritoid (ct): $[Fe,Mg]Al_2SiO_5(OH)_2$

A symmetric solution model is used for Mg–Fe mixing in binary chloritoid with the interaction parameter W(mct, fct) = 1·0 kJ/mol following Holland & Powell (1998). End-members:

Mg-chloritoid (mct): $MgAl_2SiO_5(OH)_2$;
Fe-chloritoid (fct): $FeAl_2SiO_5(OH)_2$.

Downloaded from http://petrology.oxfordjournals.org/ at Pennsylvania State University on March 5, 2016

Carpholite (cr): $[Fe,Mg]Al_2Si_2O_6(OH)_4$
Mg–Fe mixing in carpholite is assumed to be ideal. End-members:

Mg-carpholite (mcr): $MgAl_2Si_2O_6(OH)_4$;
Fe-carpholite (fcr): $FeAl_2Si_2O_6(OH)_4$.

Chlorite (chl): $[Fe,Mg,]_4^{M2,3}[Mg,Fe,Al]_2^{M1,4}[Si,Al]_2^{T1}Si_2^{T2}O_{10}(OH)_8$
According to Holland *et al.* (1998), the thermodynamics of ordered chlorite are modelled using a quaternary symmetric mixing model. End-members:

Al-free chlorite (afchl): $[Mg]_4^{M2,3}[Mg]^{M1}[Mg]^{M4}[Si]_2^{T1}[Si]_2^{T2}O_{10}(OH)_8$;
clinochlore (clin): $[Mg]_4^{M2,3}[Mg]^{M1}[Al]^{M4}[Al]^{T1}[Si]^{T1}[Si]_2^{T2}O_{10}(OH)_8$;
daphnite (daph): $[Fe]_4^{M2,3}[Fe]^{M1}[Al]^{M4}[Al]^{T1}[Si]^{T1}[Si]_2^{T2}O_{10}(OH)_8$;
amesite (ames): $[Mg]_4^{M2,3}[Al]^{M1}[Al]^{M4}[Al]_2^{T1}[Si]_2^{T2}O_{10}(OH)_8$.

Interaction parameters: W(afchl, clin) = 18 kJ/mol, W(afchl, daph) = 14·5 kJ/mol, W(afchl, ames) = 20 kJ/mol, W(clin, daph) = 2·5 kJ/mol, W(clin, ames) = 18 kJ/mol and W(daph, ames) = 13·5 kJ/mol.

Phengite (ph): $K\square^{M1}[Fe,Mg,Al]^{M2A}[Al]^{M2B}[Si,Al]_2^{T1}Si_2^{T2}O_{10}(OH)_2$
Following Holland & Powell (1998), an ideal mixing model is used for phengite where mixing between Al, Mg and Fe is assumed only to occur in the M2A site and mixing of tetrahedral Al and Si is restricted to the two T1 sites. End-members:

muscovite (mu): $K\square^{M1}[Al]^{M2A}[Al]^{M2B}Al^{T1}Si^{T1}Si_2^{T2}O_{10}(OH)_2$;
celadonite (cel): $K\square^{M1}[Mg]^{M2A}[Al]^{M2B}Si_2^{T1}Si_2^{T2}O_{10}(OH)_2$;
Fe-celadonite (fcel): $K\square^{M1}[Fe]^{M2A}[Al]^{M2B}Si_2^{T1}Si_2^{T2}O_{10}(OH)_2$.

Biotite (bi): $K[Fe,Mg]_2^{M2}[Fe,Mg,Al]^{M1}[Si,Al]_2^{T1}Si_2^{T2}O_{10}(OH)_2$
Following Powell & Holland (1999), ordered biotite is modelled with symmetric mixing and DQF models where Fe is assumed to favour the M1 site. End-members:

phlogopite (phl): $K[Mg]_2^{M2}[Mg]^{M1}Al^{T1}Si^{T1}Si_2^{T2}O_{10}(OH)_2$;
annite (ann): $K[Fe]_2^{M2}[Fe]^{M1}Al^{T1}Si^{T1}Si_2^{T2}O_{10}(OH)_2$;
eastonite (east): $K[Mg]_2^{M2}[Al]^{M1}Al_2^{T1}Si_2^{T2}O_{10}(OH)_2$;
ordered-biotite (obi): $K[Mg]_2^{M2}[Fe]^{M1}Al^{T1}Si^{T1}Si_2^{T2}O_{10}(OH)_2$.

Interaction parameters: W(phl, ann) = 9 kJ/mol, W(phl, east) = 10 kJ/mol, W(phl, obi) = 3 kJ/mol, W(ann, east) = −1 kJ/mol, W(ann, obi) = 6 kJ/mol, W(east, obi) = 10 kJ/mol, and a DQF parameter, I_{obi} = −10·73 kJ/mol.

Talc (ta): $[Fe,Mg]_2^{M1}[Fe,Mg,Al]^{M3}[Si,Al]_2^{T1}[Si]_2^{T2}O_{10}(OH)_2$
Following Holland & Powell (1998), an ideal mixing model is used for the ternary talc in which the Al is assumed to order onto the M3 site and to enter only the two T1 sites. End-members:

talc (ta): $[Mg]_2^{M1}[Mg]^{M3}[Si]_2^{T1}[Si]_2^{T2}O_{10}(OH)_2$;
Fe-talc (fta): $[Fe]_2^{M1}[Fe]^{M3}[Si]_2^{T1}[Si]_2^{T2}O_{10}(OH)_2$;
Tschermak-talc (tats): $[Mg]_2^{M1}[Al]^{M3}[Al]^{T1}[Si]^{T1}[Si]_2^{T2}O_{10}(OH)_2$.

Staurolite (st): $[Fe,Mg]_4Al_{18}Si_{7.5}O_{44}(OH)_4$
A symmetric solution model is used for Mg–Fe mixing in binary staurolite with the interaction parameter W(mst, fst) = −8·0 kJ/mol following White *et al.* (2001). End-members:

Mg-staurolite (mst): $Mg_4Al_{18}Si_{7.5}O_{44}(OH)_4$;
Fe-staurolite (fst): $Fe_4Al_{18}Si_{7.5}O_{44}(OH)_4$.

Glaucophane (gl): $Na_2[Mg,Fe]_3Al_2Si_8O_{22}(OH)_2$
Fe–Mg mixing in glaucophane is assumed to be ideal. End-members:

glaucophane (gl): $Na_2Mg_3Al_2Si_8O_{22}(OH)_2$;
Fe-glaucophane (fgl): $Na_2Fe_3Al_2Si_8O_{22}(OH)_2$.

Albite (ab): $NaAlSi_3O_8$
According to Holland & Powell (1996), ordered albite is modelled with a simplified model between two end-members, low albite (abl) and high albite (abh), in which Al is assumed to order onto just one of the four tetrahedral sites. The mixing is assumed to be symmetric with W(ab) = 13·45 + 0·036 P and a DQF parameter $I_{abh} = -14 + 0{\cdot}0187\,T - 0{\cdot}036\,P$.

Single end-member minerals with unit activities are:

Paragonite (pa): $NaAl_2(AlSi_3)O_{10}(OH)_2$
Jadeite (jd): $NaAlSi_2O_6$
Kyanite (ky) and sillimanite (sill): Al_2SiO_5
Quartz (q) and coesite (coe): SiO_2.

Downloaded from http://petrology.oxfordjournals.org/ at Pennsylvania State University on March 5, 2016